

AD-771 148

ESTIMATION OF THE STATIC AERODYNAMIC
CHARACTERISTICS OF ORDNANCE PROJECTILES
AT SUPERSONIC SPEEDS

Robert L. McCoy

Ballistic Research Laboratories
Aberdeen Proving Ground, Maryland

November 1973

DISTRIBUTED BY:

NTIS

National Technical Information Service
U. S. DEPARTMENT OF COMMERCE
5285 Port Royal Road, Springfield Va. 22151

UNCLASSIFIED
Security Classification

AD-771148

DOCUMENT CONTROL DATA - R & D

(Security classification of title, body of abstract and indexing annotation must be entered when the overall report is classified)

1. ORIGINATING ACTIVITY (Corporate author) U. S. Army Ballistic Research Laboratories Aberdeen Proving Ground, Maryland 21005		2a. REPORT SECURITY CLASSIFICATION Unclassified	
		2b. GROUP	
3. REPORT TITLE ESTIMATION OF THE STATIC AERODYNAMIC CHARACTERISTICS OF ORDNANCE PROJECTILES AT SUPERSONIC SPEEDS			
4. DESCRIPTIVE NOTES (Type of report and inclusive dates)			
5. AUTHOR(S) (First name, middle initial, last name) Robert L. McCoy			
6. REPORT DATE NOVEMBER 1973		7a. TOTAL NO. OF PAGES 76 69	7b. NO. OF REFS 25
8a. CONTRACT OR GRANT NO. a. PROJECT NO. RDT&E 1T562603A041 c. d.		8b. ORIGINATOR'S REPORT NUMBER(S) BRL REPORT NO. 1682	
8c. OTHER REPORT NUMBER(S) (Any other numbers that may be assigned this report)			
10. DISTRIBUTION STATEMENT Approved for public release; distribution unlimited.			
11. SUPPLEMENTARY NOTES		12. SPONSORING MILITARY ACTIVITY U. S. Army Materiel Command 5001 Eisenhower Avenue Alexandria, Virginia 22304	
13. ABSTRACT <p>A simplified flow field solution has been programmed in an attempt to improve the accuracy of estimates of the static aerodynamic characteristics of ordnance projectiles. It provides estimates of drag, normal force, static moment, and roll damping moment for pointed bodies of revolution at supersonic speed. The program combines the Van Dyke hybrid theory for potential flow, the Van Driest compressible turbulent boundary layer theory, and the Chapman-Sternberg model for supersonic base pressure. Good agreement is demonstrated between the theoretical and experimental data.</p>			

Reproduced by
NATIONAL TECHNICAL
INFORMATION SERVICE
U S Department of Commerce
Springfield VA 22151

DD Form 1473
1 NOV 66

REPLACES DD FORM 1473, 1 JAN 64, WHICH IS
OBSOLETE FOR ARMY USE.

UNCLASSIFIED

Security Classification

UNCLASSIFIED

Security Classification

14. KEY WORDS	LINK A		LINK B		LINK C	
	ROLE	WT	ROLE	WT	ROLE	WT
Supersonic Potential Flow Boundary Layer Corrections Drag Normal Force Pitching Moment						

11

UNCLASSIFIED

Security Classification

Destroy this report when it is no longer needed.
Do not return it to the originator.

Secondary distribution of this report by originating
or sponsoring activity is prohibited.

Additional copies of this report may be obtained
from the National Technical Information Service,
U.S. Department of Commerce, Springfield, Virginia
22151.

ACCESSION for	
NTIS	With Section <input checked="" type="checkbox"/>
DOC	With Section <input type="checkbox"/>
UNCLASSIFIED	<input type="checkbox"/>
JUSTIFICATION	
BY	
DISTRIBUTION/AVAILABILITY CODES	
DISL	A ALL USE/SPECIAL
A	

The findings in this report are not to be construed as
an official Department of the Army position, unless
so designated by other authorized documents.

///

BALLISTIC RESEARCH LABORATORIES

REPORT NO. 1682

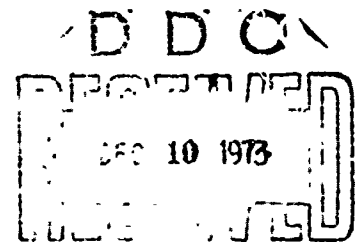
NOVEMBER 1973

**ESTIMATION OF THE STATIC AERODYNAMIC CHARACTERISTICS
OF ORDNANCE PROJECTILES AT SUPERSONIC SPEEDS**

Robert L. McCoy

Exterior Ballistics Laboratory

Approved for public release; distribution unlimited.



RDT&E Project No. 1T562603A041

ABERDEEN PROVING GROUND, MARYLAND

1

BALLISTIC RESEARCH LABORATORIES

REPORT NO. 1682

RLMcCoy/ajb
Aberdeen Proving Ground, Md.
November 1973

ESTIMATION OF THE STATIC AERODYNAMIC CHARACTERISTICS
OF ORDNANCE PROJECTILES AT SUPERSONIC SPEEDS

ABSTRACT

A simplified flow field solution has been programmed in an attempt to improve the accuracy of estimates of the static aerodynamic characteristics of ordnance projectiles. It provides estimates of drag, normal force, static moment, and roll damping moment for pointed bodies of revolution at supersonic speed. The program combines the Van Dyke hybrid theory for potential flow, the Van Driest compressible turbulent boundary layer theory, and the Chapman-Sternberg model for supersonic base pressure. Good agreement is demonstrated between the theoretical and experimental data.

TABLE OF CONTENTS

	Page
ABSTRACT	3
LIST OF ILLUSTRATIONS	7
LIST OF SYMBOLS	9
I. INTRODUCTION	13
II. METHOD OF SOLUTION OF THE FLOW FIELD AROUND A PROJECTILE	14
A. Potential Flow	14
B. Viscosity Correction	15
III. SOLUTION OF THE POTENTIAL FLOW.	16
IV. SKIN FRICTION EFFECTS.	19
V. ESTIMATION OF BASE DRAG	21
VI. CORRECTION FOR A BOUNDARY LAYER DISPLACEMENT THICKNESS	24
VII. COMPARISON OF THE PRESENT THEORY WITH EXPERIMENTAL RESULTS.	26
VIII. COMMENTS ON SMALL ARMS AND ARTILLERY PROCEDURES	28
A. Small Arms Projectiles	29
B. Artillery Projectiles	31
IX. CONCLUSIONS	32
ACKNOWLEDGEMENT	34
REFERENCES	53
APPENDIX	57
DISTRIBUTION LIST	71

LIST OF ILLUSTRATIONS

Figure		Page
1.	Pressure Coefficient on a Cone	35
2.	Normal Force Slope for a Cone	36
3.	Pressure Ratio Along a Boattailed Cone Cylinder Projectile	37
4.	Pressure Ratio Along a Boattailed Cone Cylinder Projectile	38
5.	Pressure Ratio Along a Boattailed Projectile.	39
6.	Ratio of Base Pressure to Local Static Pressure vs. Mach Number	40
7.	Normal Force Slope vs. Mach Number	41
8.	Normal Force Center of Pressure vs. Mach Number	42
9.	Zero-Yaw Drag Coefficient vs. Mach Number	43
10.	Normal Force Coefficient vs. Mach Number	44
11.	Static Moment Coefficient vs. Mach Number	45
12.	Roll Damping Moment Coefficient vs. Mach Number	46
13.	Drag, Normal Force, and Static Moment Coefficients vs. Mach Number	47
14.	Drag, Normal Force, and Static Moment Coefficients vs. Mach Number	48
15.	Drag, Normal Force, and Center of Pressure vs. Boattail Angle.	49
16.	Drag, Normal Force, and Static Moment Coefficients vs. Mach Number	50
17.	Ratio of Experimental to Theoretical Drag, Normal Force, and Center of Pressure for Square Based Models	51

LIST OF ILLUSTRATIONS (continued)

Figure		Page
18	Ratio of Experimental to Theoretical Drag, Normal Force, and Center of Pressure for Boattailed Models.	52

LIST OF SYMBOLS

c	Speed of sound
c_o	Speed of sound in the free stream
C_{FT}	Turbulent skin friction coefficient
C_p	Pressure coefficient
C_{P_o}	Pressure coefficient at zero angle of attack
C_{P_1}	Cross flow pressure coefficient
C_{D_o}	Total drag coefficient at zero angle of attack
C_{DP}	Pressure drag coefficient
C_{DSF}	Skin friction drag coefficient
C_{DB}	Base drag coefficient
C_{L_p}	Roll damping moment coefficient
C_{M_α}	Static moment slope at zero angle of attack
C_{N_α}	Normal force slope at zero angle of attack
d	Reference diameter of projectile
d_B	Base diameter of projectile
$f(\xi)$	Local axial source strength at axial location ξ
$g(\xi)$	Local doublet strength at axial location ξ
l	Length of projectile
L	Fineness ratio (l/d)
M	Free stream Mach number
M_e	Effective Mach number at projectile base
M_B	Local Mach number at projectile base
p	Missile rolling velocity

LIST OF SYMBOLS (continued)

p	Local pressure
p_1	Free stream static pressure
p'	Local static pressure just upstream of base
p_t	Total pressure
p_B	Base pressure
q	Total perturbation velocity
r	Radial distance in cylindrical coordinate system
R	Local body radius
R'	Local body slope
$()_r$	Indicates partial differentiation with respect to r
Re_L	Reynolds number, based on missile length
S_W	Wetted surface area of projectile
t	Ratio of tangent of polar angle to tangent of Mach angle
u	Axial perturbation velocity
U	Free stream speed
v	Radial perturbation velocity
w	Azimuthal perturbation velocity
x	Axial distance from nose of projectile
$()_x$	Indicates partial differentiation with respect to x
X_{CPN}	Normal force center of pressure, from projectile nose
α	Angle of attack
β	$\sqrt{M^2 - 1}$, cotangent of free stream Mach angle
γ	Ratio of specific heats
δ	Step size for potential flow calculation
δ_i	Incompressible boundary layer thickness

LIST OF SYMBOLS (continued)

δ_c	Compressible boundary layer thickness
δ^*	Displacement thickness
ϵ	Body thickness ratio
θ	Azimuthal angle in cylindrical coordinate system
$()_\theta$	Indicates partial differentiation with respect to θ
λ	Compressibility parameter in turbulent skin friction calculation
ν	Prandtl Meyer angle
ξ	Axial location of a source, sink, or doublet in potential flow
ρ	Density of air
ϕ_0	First order axial flow potential
ϕ_1	First order cross flow potential
ϕ_0	Second order axial flow potential
ψ	Exact perturbation potential
λ_0	Auxiliary first order potential used in second order solution
γ_0	Van Dyke's particular solution
ψ	Velocity potential
ω	Power law viscosity coefficient

I. INTRODUCTION

For several years the Exterior Ballistics Laboratory of the Ballistics Research Laboratories has been engaged in an attempt to improve the accuracy of estimates of the aerodynamic characteristics of projectiles. Some fairly good semi-empirical methods for bodies of revolution have been used in the past, such as Hitchcock's method^{1*} of estimating aerodynamic drag; the Wood-Simmons method^{2, 3} for normal force and static moment; and the Wood-Murphy unsteady slender body theory⁴ which includes estimates of pitch damping derivatives. In addition, a totally empirical method called "Spinner" has recently been advanced by Whyte⁵. This method utilizes the large memory of a digital computer to store the experimentally determined aerodynamic characteristics of many existing projectile designs. A table search combined with a multiple interpolation routine is then used to estimate the unknown characteristics for a given configuration. The "Spinner" method appears to be reasonably accurate for projectiles which do not differ appreciably from one or more of those tabulated in the data bank.

Although the methods in current use are capable of providing quick and fairly accurate estimates of aerodynamic characteristics for most projectiles of conventional design, the recent advent of large scale, high speed computing machinery has prompted a re-examination of the more fundamental approach to the problem - that of computational fluid dynamics. This report compares the results of a simplified flow field solution with results obtained experimentally for one class of projectiles (pointed bodies at small static angle of attack in supersonic flow) and indicates some areas in which improvement of the simplified fluid model are needed. (An analogous flowfield solution has recently been published by Moore²⁶.)

*References are listed on page 53.

II. METHOD OF SOLUTION OF THE FLOW FIELD AROUND A PROJECTILE

A. Potential Flow

For the prediction of static aerodynamic characteristics, the projectile is assumed to be a rigid, reasonably slender, pointed body of revolution, at small static angle of attack in uniform supersonic flow. The flow is assumed to be inviscid, irrotational, isentropic, and everywhere supersonic (the restriction to "low supersonic" speed avoids the essential non-linearity of transonic flow). Under these assumptions, the fluid velocity can be expressed as the gradient of a potential field, and the solution of the potential flow around the projectile represents a first approximation of the real flow field.

At moderate supersonic speeds and small angles of attack, the most serious omission made in this first approximation is the neglect of viscosity. No significant regions of separated flow can be accounted for in an inviscid theory; in particular, the large separated flow region aft of a blunt base requires a special treatment of base effects. Another important omission in the theory is the neglect of the boundary layer. Fortunately, the stated problem deals primarily with slender bodies of revolution at high Reynolds numbers, a combination of conditions for which classical boundary layer theory is applicable. The principal, direct effects of the boundary layer are to add skin friction and to slightly modify the direction of the streamlines close to the surface. The boundary layer also has an indirect effect on the base pressure, since the flow in the near wake depends on local flow conditions just upstream of the base. Therefore, the addition of a boundary layer solution represents a second approximation to the real flow field.

The specific theory selected for solution of the potential flow field was Van Dyke's hybrid theory^{6,7} which combines a second-order axial solution with a first-order approximation for the cross flow. This method is computationally faster by a factor of 1000 than an equivalent

solution by the method of characteristics. For typical slender projectile designs at moderate supersonic speeds, disagreement with a solution by characteristics is usually less than 2% in velocity and pressure.

B. Viscosity Corrections

The skin friction effect for compressible turbulent boundary layers on flat plates has been investigated by Van Driest⁸, and his theory was used to estimate skin friction effects on drag and roll damping moment. The effect of the boundary layer on the flow field adjacent to the surface of the body is accounted for by adding the local displacement thickness to the local bare-body radius, and solving the inviscid flow field with an adjusted boundary condition. A boundary layer solution could be formally introduced, but would significantly complicate the calculation; because of the approximate nature of the correction, a linear variation of boundary layer displacement thickness was assumed as a concession to the computing scheme. The turbulent flat plate boundary layer displacement thickness at the projectile base is estimated; at the nose, the thickness is assumed to be zero; then the local displacement thickness is assumed to vary linearly with axial distance between the projectile nose and the base. The aerodynamic forces and moments are then determined for the bare-body plus the linear displacement thickness.

The addition of an estimate of the turbulent base pressure completes the required component parts for a free-flight total drag estimate. The base pressure estimate used consists of a combination of the method of Chapman⁹ for square based projectiles and Sternberg's correction¹⁰ for boattails. This simple semi-empirical base pressure estimate appears to work fairly well, except for boattails at low supersonic speeds.

The adverse pressure gradient over a boattail markedly thickens the turbulent boundary layer in that region; hence the flat plate equation underestimates boundary layer thickness at the base of a boattailed

shell (the flow can also separate along a boattail). Chapman⁹ found that thickening the boundary layer lowers base pressure and increases base drag. The effect of using the flat plate boundary layer thickness for boattailed configurations is to underestimate the base drag. The normal force and static moment estimates are also affected by the error in displacement thickness along the boattail, although the effect on the cross flow is weaker than the effect on velocities in the near wake.

III. SOLUTION OF THE POTENTIAL FLOW

The axial flow around the projectile is solved to first order by superposition of the five basic solutions stated in the Appendix, equations (A. 29) through (A. 33). The first order solution and its first partial derivatives are then substituted in equation (A. 26), and the particular integral, Ψ_0 , is evaluated. The second order problem is now reduced to an equivalent first order problem, since the second order solution can be expressed as the sum of the particular integral and a complementary solution of the first order potential denoted by χ_0 ,

$$\chi_0_{rr} + \chi_0_r / r - \beta^2 \chi_0_{xx} = 0 \quad (1)$$

which is precisely the first order equation. The boundary conditions are (see equation A. 39)

$$\chi_0(0, r) = \chi_0_x(0, r) = 0 \quad (2)$$

$$\chi_0_r(x, R) = R'(1 + \varphi_0_x) - \Psi_0_r \quad (3)$$

The complementary solution χ_0 , is obtained by superposition of the same five basic solutions initially used to obtain ϕ_0 . The complete second order potential for the axial flow, ϕ_0 , is now given by,

$$\phi_0 = \psi_0 + \chi_0 \quad (4)$$

The cross flow is solved to first order by superposition of the two basic solutions, stated in the Appendix, equations (A. 35) and (A. 36). The first partial derivatives of the second order axial solution and the first order cross flow solution give the potential axial and cross flow velocities needed to determine the pressure distribution on the projectile.

The pressure coefficient, C_p , for steady, isentropic flow is given by,

$$C_p(x, r, \theta) = \frac{2}{\gamma M^2} \left\{ \left[1 + \frac{\gamma-1}{2} M^2 \left(1 - \frac{q^2}{U^2} \right) \right]^{\gamma/(\gamma-1)} - 1 \right\} \quad (5)$$

$$\text{where } \frac{q^2}{U^2} = \left(\frac{u}{U} \right)^2 + \left(\frac{v}{U} \right)^2 + \left(\frac{w}{U} \right)^2 \quad (6)$$

Substituting equation (A. 21) from the Appendix into (A. 4), (5) and (6), and expanding in series gives,

$$C_p(x, r, \theta) = C_{p_0}(x, r) \cos \alpha + C_{p_1}(x, r) \sin \alpha \cos \theta + \dots \quad (7)$$

For small angle of attack, $\sin \alpha \approx \alpha$ and $\cos \alpha \approx 1$, and equation (7) reduces to,

$$C_p(x, r, \theta) = C_{p_0}(x, r) + C_{p_1}(x, r) \alpha \cos \theta + \dots \quad (8)$$

$$\text{where } C_{P_0}(x, r) = \frac{2}{\gamma M^2} \left[\left\{ 1 + \frac{\gamma-1}{2} M^2 [1 - (1 + \phi_{0_x})^2 - \phi_{0_r}^2] \right\}^{\gamma/(\gamma-1)} - 1 \right] \quad (9)$$

$$C_{P_1}(x, r) = -2 \left[(1 + \phi_{0_x}) \phi_{1_x} + (1 + \phi_{1_r}) \phi_{0_r} \right] \left[1 + \frac{\gamma M^2}{2} C_{P_0}(x, r) \right]^{\frac{1}{\gamma}}$$

where ϕ_0 is the solution for the axial flow, and ϕ_1 is the crossflow solution.

On the surface of the projectile, equations (9) simplify to,

$$C_{P_0}(x, R) = \frac{2}{\gamma M^2} \left[\left\{ 1 + \frac{\gamma-1}{2} M^2 [1 - (1 + R'^2)(1 + \phi_{0_x})^2] \right\}^{\gamma/(\gamma-1)} - 1 \right] \quad (10)$$

$$C_{P_1}(x, R) = -2 (1 + R'^2) (1 + \phi_{0_x}) \phi_{1_x} \left[1 + \frac{\gamma M^2}{2} C_{P_0}(x, R) \right]^{\frac{1}{\gamma}}$$

The pressure drag coefficient, C_{DP} , the normal force derivative, C_{N_α} , and the normal force center of pressure, X_{CPN} (calibers from apex) are given by

$$C_{DP} = \frac{8}{d^2} \int_0^l R(x) R'(x) C_{P_0}(x) dx \quad (11)$$

$$C_{N_\alpha} = \frac{4}{d^2} \int_0^l -R(x) C_{P_1}(x) dx \quad (12)$$

$$X_{CPN} = \frac{4}{C_{N_\alpha} d^2} \int_0^l -x R(x) C_{P_1}(x) dx \quad (13)$$

where "d" is the reference diameter of the projectile and, "l" is the length.

Comparison of Van Dyke's hybrid theory with exact solutions is made in Figures 1 through 5. Figures 1 and 2 show the comparison with conical flow for pressure coefficients at zero angle of attack, and the normal force derivatives for ten degree half-angle cones. Figure 3 compares the ratio of local pressure to free stream static pressure, $(p/p_1 = 1 + \frac{1}{2} \gamma M^2 C_{p_0})$, for the second order theory and a characteristic solution, along a slender cone-cylinder-boattail design, at two supersonic speeds. Figure 4 is a representation of the calculated pressure distribution along a more blunt cone-cylinder-boattail design. Figure 5 depicts the comparison in pressure distribution along an initial cone-tangent ogive combination, followed by a cylindrical section, and several boattail angles. In general, the agreement is quite good for slender configurations at moderate supersonic speeds.

IV. SKIN FRICTION EFFECTS

Van Driest⁸ has derived an estimate of the turbulent skin friction on an insulated flat plate,

$$\frac{0.242}{\sqrt{C_{FT}}} \left(\frac{\sin^{-1} \lambda}{\lambda} \right) \sqrt{1 - \lambda^2} = \log_{10} Re_{\ell} C_{FT} + \frac{1}{2} (1 + 2\omega) \log_{10} (1 - \lambda^2), \quad (14)$$

where $1 - \lambda^2 = \left[1 + \frac{1}{2} (\gamma - 1) M^2 \right]^{-1}$

C_{FT} = Turbulent skin friction coefficient

Re_{ℓ} = Reynolds number, based on length

γ = ratio of specific heats (1.4 for air)

ω = power law viscosity exponent (0.76 for air)

M = free stream Mach number

This formula is used in the present theory, even though real projectiles are known to have heat transfer to the surface.

The wetted surface area of the projectile, S_W , is,

$$S_W = 2 \pi \int_0^L R(x) \sqrt{1 + [R'(x)]^2} dx \quad (15)$$

Equation (14) is now solved for C_{FT} by iteration, and the skin friction drag coefficient is given by,

$$C_{D_{SF}} = \frac{4}{\pi} S_W C_{FT} \quad (16)$$

For a spinning body of revolution, Charters and Kent¹¹ derived a relation between the roll damping moment coefficient, C_{L_P} , and the skin friction drag coefficient, $C_{D_{SF}}$. The relation is,

$$C_{L_P} = -\frac{1}{4} C_{D_{SF}} \quad (17)$$

where

$$C_{L_P} = \frac{\text{Roll Damping Moment}}{\frac{1}{2} \rho U^2 \left(\frac{\pi d^3}{4}\right) \left(\frac{\rho d}{V}\right)}$$

It is difficult to estimate the absolute accuracy of the skin friction drag calculation. For most ordnance projectiles at supersonic speeds, skin friction drag amounts to less than 30% of total drag; hence a reasonable error in $C_{D_{SF}}$ (say, 10%) contributes only 3% total drag error. Available free flight data for the roll damping moment agree with the estimated value from equations (16) and (17). Since no direct experimental check on the accuracy of skin friction drag is available, the agreement of the roll damping estimate with experiment provides the only evidence that the turbulent skin friction estimate is satisfactory.

V. ESTIMATION OF BASE DRAG

An estimate of the turbulent axisymmetric base pressure for ordnance projectiles is obtained from a combination of Chapman's semi-empirical method⁹ for square base designs, and Sternberg's correction¹⁰ for boattails. Chapman's model assumes that the base pressure depends on the approach Mach number at the base, and the ratio of boundary layer thickness at the base to base diameter. Most ordnance projectiles have fully turbulent boundary layers, and the Chapman model states that the base pressure data should correlate with $(L/Re_\ell^{1/5})$, the fineness ratio divided by the one-fifth power of the Reynolds number (based on length), and also with the effective Mach number of the approach flow at the base. The ratio of base pressure to local static pressure for square base projectiles can be written,

$$\frac{P_B}{P'} = f(M_e, L/Re_\ell^{1/5}) \quad (18)$$

The actual nature of the dependence of base pressure on approach Mach number and boundary layer thickness must be determined experimentally. A rather large amount of high quality free flight total drag data was available at BRL from the firings of various models through the spark photography ranges. Charters and Turetsky¹² demonstrated two techniques for obtaining base pressure from free flight data; one, the total drag subtraction method, and, two, a base pressure determination from measurement of the wake angle at the projectile base. Total drag data for cones, cone-cylinders, Army-Navy spinner rocket models, and tangent ogive-cylinders are available^{13, 14, 15, 16}.

This data was reduced for base pressure by the methods of Reference 12. Wherever possible the total drag subtraction method and the wake angle methods were compared; in all cases, agreement to within 10% error in base pressure was obtained.

The base pressure data was then analyzed to determine the nature of dependence on approach Mach number and boundary layer thickness. The final result of a least squares fitting gave the following empirical equation.

$$\frac{P_B}{P^*} = .3896 + \frac{.8964}{M_e} - \frac{.34793}{M_e^2} - .23913 M_e (L/Re_\ell)^{1/5} \quad (19)$$

with a standard error of 3.5%. This equation is valid for M_e between 1 and 3, and Re_ℓ between 10^6 and 10^8 . Figure 6 shows the first three terms of equation (19), plotted as a solid line. The plotted points are experimental values, extrapolated to $Re_\ell = \infty$, by means of the last term of equation (19).

For square base projectiles, the effective approach Mach number is simply the local Mach number just upstream of the base, which is readily determined from the potential flow solution. For boattail designs, Sternberg's correction¹⁰ defines the effective Mach number as the Mach number of parallel flow which would reach the local Mach number at the boattail base, if expanded to the surface angle two dimensionally. Since the flow is assumed to be everywhere isentropic, the effective Mach number can be calculated using the Prandtl-Meyer function.

The Prandtl-Meyer angle corresponding to the local Mach number at the base, M_B , is given by,

$$\nu_B = \sqrt{\frac{\gamma+1}{\gamma-1}} \tan^{-1} \sqrt{\frac{\gamma-1}{\gamma+1} (M_B^2 - 1)} - \tan^{-1} \sqrt{M_B^2 - 1} \quad (20)$$

The effective Mach number has a corresponding Prandtl-Meyer angle given by,

$$v_e = v_B + \tan^{-1} (R_B') \quad (21)$$

where R_B' is the meridian slope at the base of the projectile. The effective Mach number is related to the effective expansion angle by,

$$v_e = \sqrt{\frac{\gamma+1}{\gamma-1}} \tan^{-1} \sqrt{\frac{\gamma-1}{\gamma+1} (M_e^2 - 1)} - \tan^{-1} \sqrt{M_e^2 - 1} \quad (22)$$

Equation (22) must be solved for the effective Mach number, M_e .

The ratio of local static pressure to total pressure (p'/p_t), and the ratio of free stream static pressure to total pressure (p_1/p_t) are calculated from the isentropic relations,

$$\frac{p'}{p_t} = \left(1 + \frac{\gamma-1}{2} M_e^2\right)^{-\gamma/(\gamma-1)} \quad (23)$$

$$\frac{p_1}{p_t} = \left(1 + \frac{\gamma-1}{2} M^2\right)^{-\gamma/(\gamma-1)} \quad (24)$$

The ratio of base pressure to free stream static pressure is given by,

$$\frac{P_B}{p_1} = \left[\left(\frac{p'}{p_t}\right) / \left(\frac{p_1}{p_t}\right) \right] \left(\frac{P_B}{p'}\right) \quad (25)$$

where $\left(\frac{P_B}{p'}\right)$ is obtained empirically, equation (19).

The base drag coefficient, C_{D_B} , is expressed by,

$$C_{D_B} = \frac{2}{\gamma M^2} \left(\frac{d_B}{d} \right)^2 \left[1 - \frac{p_B}{p_1} \right], \quad (26)$$

where d_B = base diameter of projectile

d = reference diameter of projectile.

The simple semi-empirical method used to estimate turbulent base pressure appears to be reasonably accurate for cylindrical or slightly flared afterbodies over the range of supersonic speeds. Sternberg's correction¹⁰ for boattails yields essentially correct results for speeds well above transonic, that is, free stream Mach numbers greater than 1.5 for slender configurations.

The primary source of error in base pressure for boattails at low supersonic speed is believed to be the marked thickening of the boundary layer over a region of adverse pressure gradient. Chapman's correlations of measured base pressures show a decrease in base pressure with increasing boundary layer thickness, and a large increase in sensitivity with decreasing Mach number. Thus the flat plate boundary layer approximation underestimates base drag for boattailed shell, with an expected increase in error at low supersonic speeds.

VI. CORRECTION FOR BOUNDARY LAYER DISPLACEMENT THICKNESS

Comparison of the potential normal force derivative and normal force center of pressure with experimental data shows a systematic error. Potential flow theory consistently underestimates both normal force slope and center of pressure, and the error increases with in-

creasing body fineness ratio. This discrepancy appears directly attributable to the presence of the boundary layer; in fact, various authors have attempted to correct classical slender body theory for the effects of boundary layer displacement thickness.

Since displacement thickness is defined as the distance by which external streamlines are shifted due to boundary layer formation,¹⁷ a slight modification of potential flow theory can be made to incorporate the displacement thickness correction. The displacement thickness is estimated along the body surface, added to the local bare-body radius, and the potential flow field is solved with the "revised" boundary condition.

Schlichting¹⁷ has derived an expression for incompressible turbulent boundary layer displacement thickness for a flat plate of length l . If we let $L = l/d$, Schlichting's Formula becomes,

$$(\delta_i^*/d)_{\text{Base}} = .046 L / \text{Re}_l^{1/5}, \quad (27)$$

where $(\delta_i^*/d)_{\text{Base}}$ is the incompressible boundary layer displacement thickness at the trailing edge, in calibers.

Van Driest⁸ has derived the effect of compressibility on turbulent boundary layer thickness. A good approximation to Van Driest's result for the ratio of compressible to incompressible thickness is,

$$(\delta_c / \delta_i) = \left[1 + .046 \left(\frac{\gamma-1}{2} \right) M^2 \right]^{.88} \quad (28)$$

Assuming that $(\delta_c / \delta_i) = (\delta_c^* / \delta_i^*)$, equations (27) and (28) can be combined to estimate compressible turbulent displacement thickness at the projectile base,

$$(\delta_c^*/d)_{\text{Base}} = \frac{.046L}{\text{Re}_l^{1/5}} \left[1 + .046 \left(\frac{\gamma-1}{2} \right) M^2 \right]^{.88} \quad (29)$$

The actual rate of growth of turbulent boundary layer thickness is proportional to $x^{4/5}$, where x is the downstream distance from the apex. However, a $4/5$ th power growth rate introduces a complication in the potential solution near the leading edge. Downstream of the leading edge, a linear boundary layer growth rate is a reasonable approximation to the $4/5$ th power law; hence a simplifying assumption was made for the benefit of the computing scheme. The displacement thickness at the projectile base is estimated from equation (29), the thickness at the leading edge is assumed to be zero, and the local thickness is constrained to vary linearly with downstream distance at intermediate locations. The effect of body shape is not taken into account for the displacement thickness estimate. No attempt is made in the present theory to include the effect of angle of attack on the boundary layer.

For the five, seven, and nine caliber Army-Navy spinner rocket configurations, Figures 7 and 8 compare the pure potential (bare-body boundary condition) normal force slope and center of pressure with theoretical values corrected for axisymmetric displacement thickness and with experimental data. The Reynolds number range for the spinner rocket models was between 3×10^6 and 10^7 , based on model length. The boundary layer correction markedly improves the accuracy of prediction, especially for the longer projectiles.

VII. COMPARISON OF THE PRESENT THEORY WITH EXPERIMENTAL RESULTS

The results of a comparison between the values obtained with the present theory and those obtained experimentally are shown in the following figures. Figures 9 through 12 present the comparison with range data¹⁵ for the Army-Navy spinner rocket configuration. The comparison in Figure 13 is with data^{13, 14} for a cone-cylinder model,

while that for Figure 14 is with unpublished range data for an idealized model of a typical square based artillery projectile. It is to be noted from these figures that the agreement between theory and experiment is quite good over the useful range of supersonic speeds.

Figure 15 compares theoretical values with measured data¹⁶ for several boattail angles at a free stream Mach number of 1.7; at this speed the agreement is good. Figure 16 shows the comparison with experimental data for an idealized model of a typical boattailed ordnance projectile. The theory considerably underestimates total drag for boattailed shell at low supersonic speeds. As indicated previously, the primary source of total drag error at such speeds is believed to be an error in the base pressure estimate. The errors in normal force and static moment slopes are much smaller, since the flat plate boundary layer displacement thickness estimate is not seriously degraded by adding a short boattail.

Estimates of drag, normal force slope and center of pressure were also calculated, using the present theory, for the additional free flight range tests reported in references 17 through 20. These models included head length variations on the Army-Navy spinner projectiles, cone-cylinders of high fineness ratio, and various boattailed configurations.

The experimental data reported in references 13 through 20 are based on free flight spark range firings of smooth, pointed, aerodynamically clean models, nominally 20 millimeters in diameter. A comprehensive comparison of this data with that obtained with the present theory is shown in Figures 17 and 18. Some of the experimental data shown in these Figures is of uncertain quality; hence a larger scatter is observed than in previous Figures.

Figure 17 depicts for square based projectiles the ratio of the experimental drag, normal force, and center of pressure to the theo-

retical estimates as plotted against free stream Mach number. Agreement between theory and experiment is good at all of the free stream Mach numbers considered, with the largest errors observed being under 10 percent.

Figure 18 is a plot similar to that presented in Figure 17 except that it is for projectiles of boattailed design. It indicates for shell of this type equally good agreement at free stream Mach numbers greater than 1.7. However at Mach 1.5 systematic errors in the theoretical values of the order of 10 percent are observed. At Mach 1.3, the errors range from 15 to 25 percent.

The stated objective in the development of the present theory is to improve the state-of-the-art in estimating the static aerodynamic characteristics of ordnance projectiles. For aerodynamically clean vehicles, Figure 17 indicates high quality estimates on square based designs. Figure 18 shows reliable results on clean boattailed designs at free stream Mach numbers greater than 1.7. If estimates are required for a boattailed design at lower supersonic speeds, the trends indicated in Figure 18 may be used to qualitatively adjust the theoretical results.

VIII. COMMENTS ON SMALL ARMS AND ARTILLERY PROJECTILES

Use of the present theory to estimate static aerodynamic characteristics of typical ordnance designs is handicapped by the fact that most real ordnance projectiles violate to some extent one or more of the physical assumptions inherent in the simplified fluid models. For a specific design, the nature of the violation can usually be classified as either basic or minor. If a given projectile basically violates the physical assumptions of the theory, the resulting estimates will be

unreliable, and in general, uncorrectable by any uniformly satisfactory method. Examples of basic violations are large thickness ratios or severe leading edge bluntness, which violate the assumption of isentropic flow; or a large region of separated flow along the projectile's surface, which invalidates the boundary layer assumption.

If a given projectile design contains only minor violations of the physical assumptions, it is usually possible to correct the theoretical estimates, at least qualitatively, for the known errors. Examples of minor violations are small leading edge bluntness (méplats), screw holes, wrench slots, bourrelets, small rings, grooves or body undercuts, shallow helical body serrations, and, at least for square based designs, small rotating bands. (In general, if a surface recess or protuberance on a projectile wall is smaller than the local boundary layer thickness at that point, the violation is considered minor.)

Small arms and artillery projectiles represent two classes of real ordnance design to which the present theory has been applied. The violations encountered with these two classes of shell are sufficiently distinct and different to warrant separate discussion.

Details of quantitative corrections for minor violations of the present theory will be published in the near future as separate reports for specific classes of ordnance projectiles.

A. Small Arms Projectiles

The conventional small arms bullet is a nearly pointed, slender body of revolution, with shallow helical serrations impressed on the cylindrical section by the rifled gun barrel. The bullet may or may not have a boattail, but due to the swaging process used in manufacture, most production bullets have rounded corners at the base. The gilding

metal jacket and the lead-antimony core are cold-formed to the prescribed design in a polished swage, and the outer contour of the bullet is generally a very smooth surface.

Conventional small arms bullets are seldom over one inch long, and at moderate supersonic speed, the free flight Reynolds number usually lies in the transition range. The combination of transition Reynolds number and a smooth surface promotes initially laminar boundary layers, with transition usually occurring somewhere on the body. The present theory assumes a fully developed turbulent boundary layer, and from the strict viewpoint of fluid physics, an initially laminar boundary layer constitutes a basic violation. However, the present theory includes boundary layer effects only as a second order correction to the potential flow field; in the mathematical sense, boundary layer transition on the body introduces only a minor violation.

Since a laminar boundary layer produces significantly less skin friction than a turbulent one, the present theory should overestimate skin friction drag for small arms bullets. However, Chapman⁹ shows that a laminar boundary layer creates lower base pressure and therefore the theory should underestimate base drag for the laminar case.

The possibility of a fortuitous cancellation of the two errors has been confirmed experimentally for several small arms bullets with predominantly laminar boundary layers. The normal force and center of pressure estimates for the same projectiles were significantly higher than experimental values, since the present theory overestimates the displacement thickness for a projectile with a laminar boundary layer.

Rounded corners at the base of a projectile cause boundary layer separation upstream of the actual base. The assumptions of potential

flow and the boundary layer are valid only in the region upstream of the separation point. If separation physically occurs close to the actual projectile base, the separation point is assumed to be the effective base location for use in the present theory. Unfortunately, no simple method exists for predicting the separation point on rounded bases. Good agreement between theoretical and experimental values has been obtained for rounded base designs when the separation point was visually determined from spark shadowgraphs.

Application of the theory to the drawing shape of a gilding metal-lead bullet can introduce additional errors in estimation because deformation of the projectile in the bore is neglected. Spark shadowgraphs of bullets in free flight often reveal a significantly different contour from that initially loaded in the gun. Errors in drag estimates as great as 20 percent have been traced to such bullet deformation, but marked improvement results when the theory is applied to the contour measured from shadowgraphs.

B. Artillery Projectiles

Typical artillery shells are characterized by fuzes with meplats, rough surfaces, screw holes and wrench slots, bourrelets, rings, grooves, body undercuts, and rotating bands, all of which tend to promote fully developed turbulent boundary layers.

The drag increase due to a small meplat can be calculated approximately and added to the theoretical estimate. The effect of rings, grooves, body undercuts and rotating bands is to add parasitic drag, which can be qualitatively estimated^{21, 22}. The effect of surface irregularities on the errors in normal force and center of pressure are difficult to estimate.

The effect of a rotating band depends on its size and location. A large band with a blunt trailing edge causes local boundary layer separation just downstream of the band, and if the flow is required to turn the expansion angle to the boattail before reattachment has occurred, the present theory is basically violated. If the band is small, or far enough forward so that reattachment occurs before the flow reaches the boattail, the principal effect of the band is simply to thicken the boattail boundary layer. In this case, the net effect of the rotating band is an accentuation of the errors shown in Figure 18, for idealized boattailed configurations. Unfortunately, even good spark shadowgraphs do not always reveal the location of boundary layer reattachment, and for the case of a rotating band upstream of a boattail, the present theory must be used with caution.

IX. CONCLUSIONS

The estimates of static aerodynamic characteristics obtained by the method outlined in this report agree with experimental results to within ten percent error, for aerodynamically clean, square based projectiles. At free stream Mach numbers above 1.5, equally good estimates are obtained for boattailed configurations. At low supersonic speeds, the present theory shows systematic errors of order of twenty percent for boattails. The error trends observed in Figure 18 for low speeds may be used to qualitatively correct the theoretical estimates for boattailed designs.

The present theory could be improved by adding a numerical solution of the axisymmetric turbulent boundary layer equations, using the pressure distribution obtained from the inviscid solution. Similarly, several authors have recently published techniques^{23, 24} for solution

of the axisymmetric turbulent wake of a supersonic projectile, including boattailed and flared afterbodies. Reference 25 gives a method of estimating base pressure for the rocket case. Future efforts involving the present theory should include studies to determine if adding more refined boundary layer and turbulent wake solutions offer significant improvement in results, at a reasonable cost in computing time.

X. ACKNOWLEDGEMENT

The author is grateful to Mr. L. C. MacAllister for providing much of the free flight range data shown in this report, and for numerous helpful suggestions on improvements to the theoretical models.

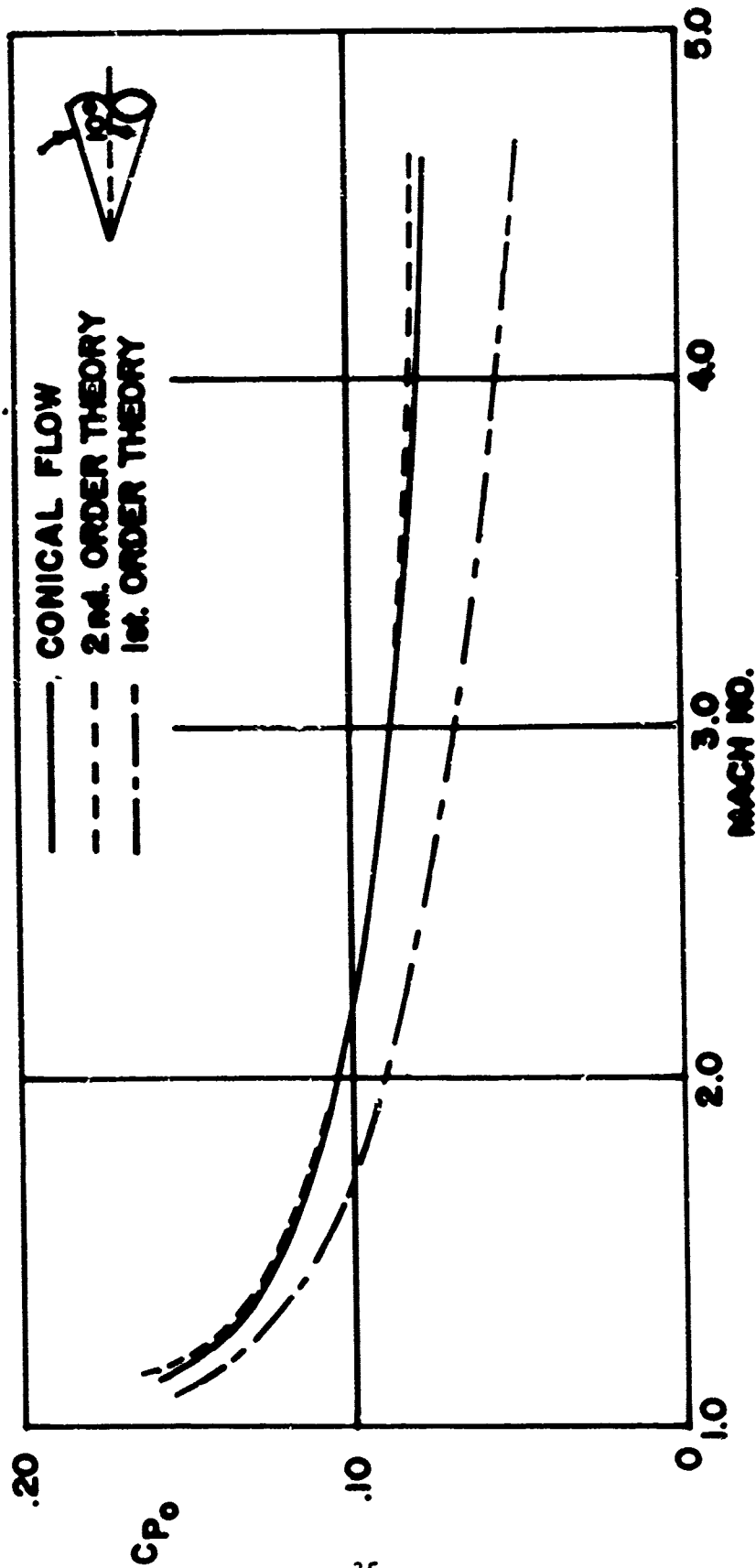


FIG.1 PRESSURE COEFFICIENT ON A CONE

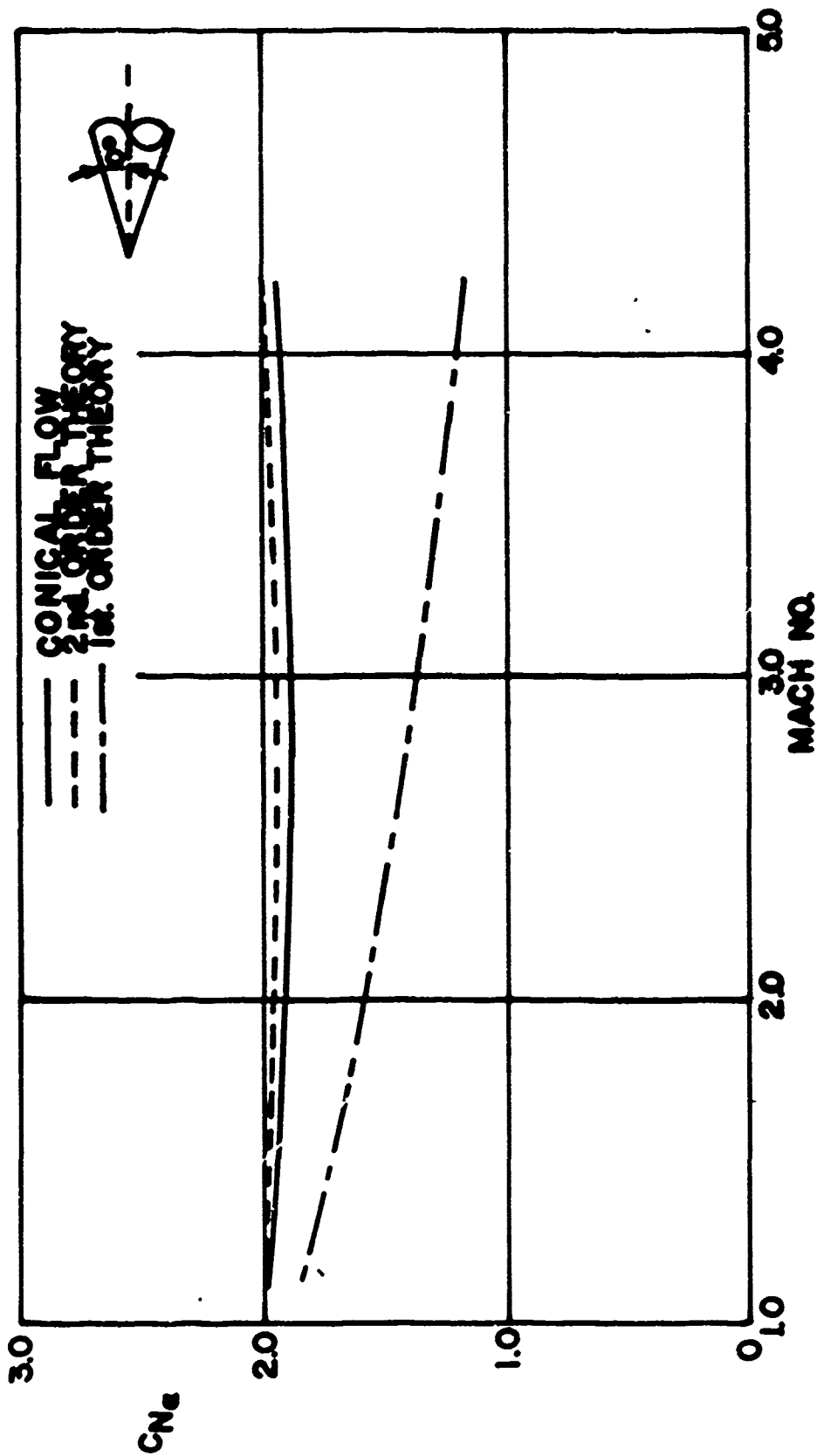


FIG.2 NORMAL FORCE SLOPE FOR A CONE

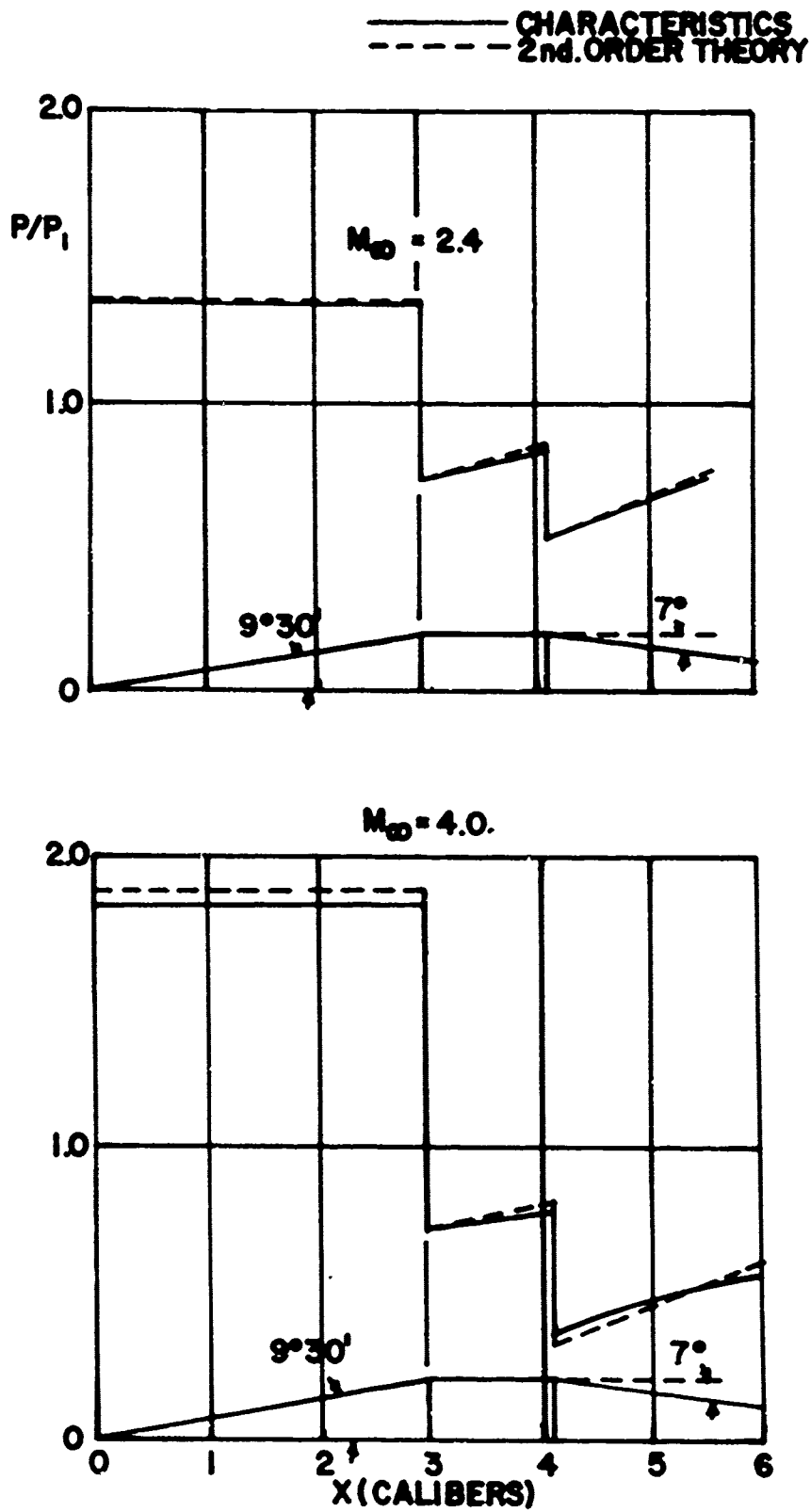
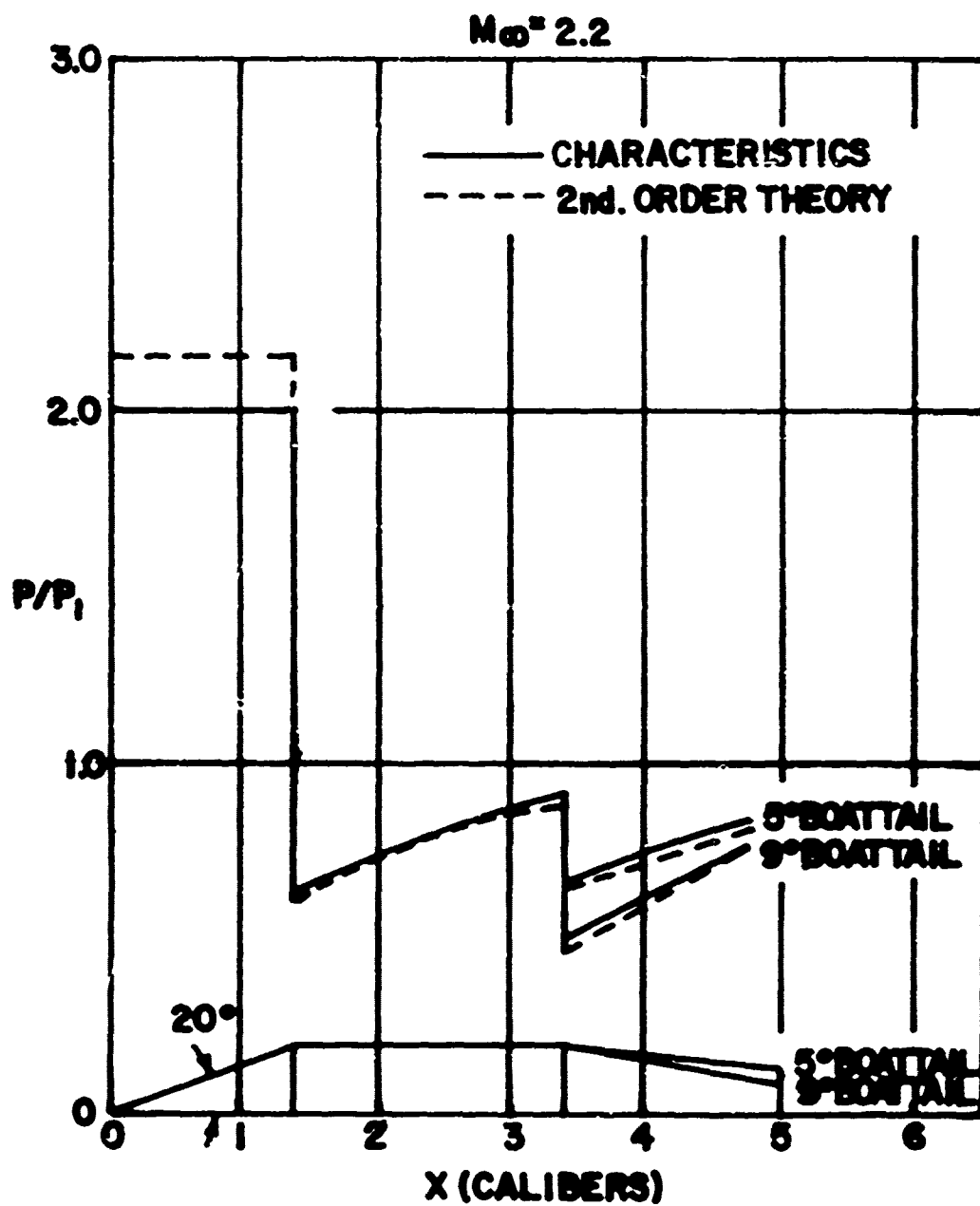


FIG.3 PRESSURE RATIO ALONG A BOAT-TAILED CONE CYLINDER PROJECTILE



**FIG. 4 PRESSURE RATIO ALONG A BOATTAILED
CONE CYLINDER PROJECTILE**

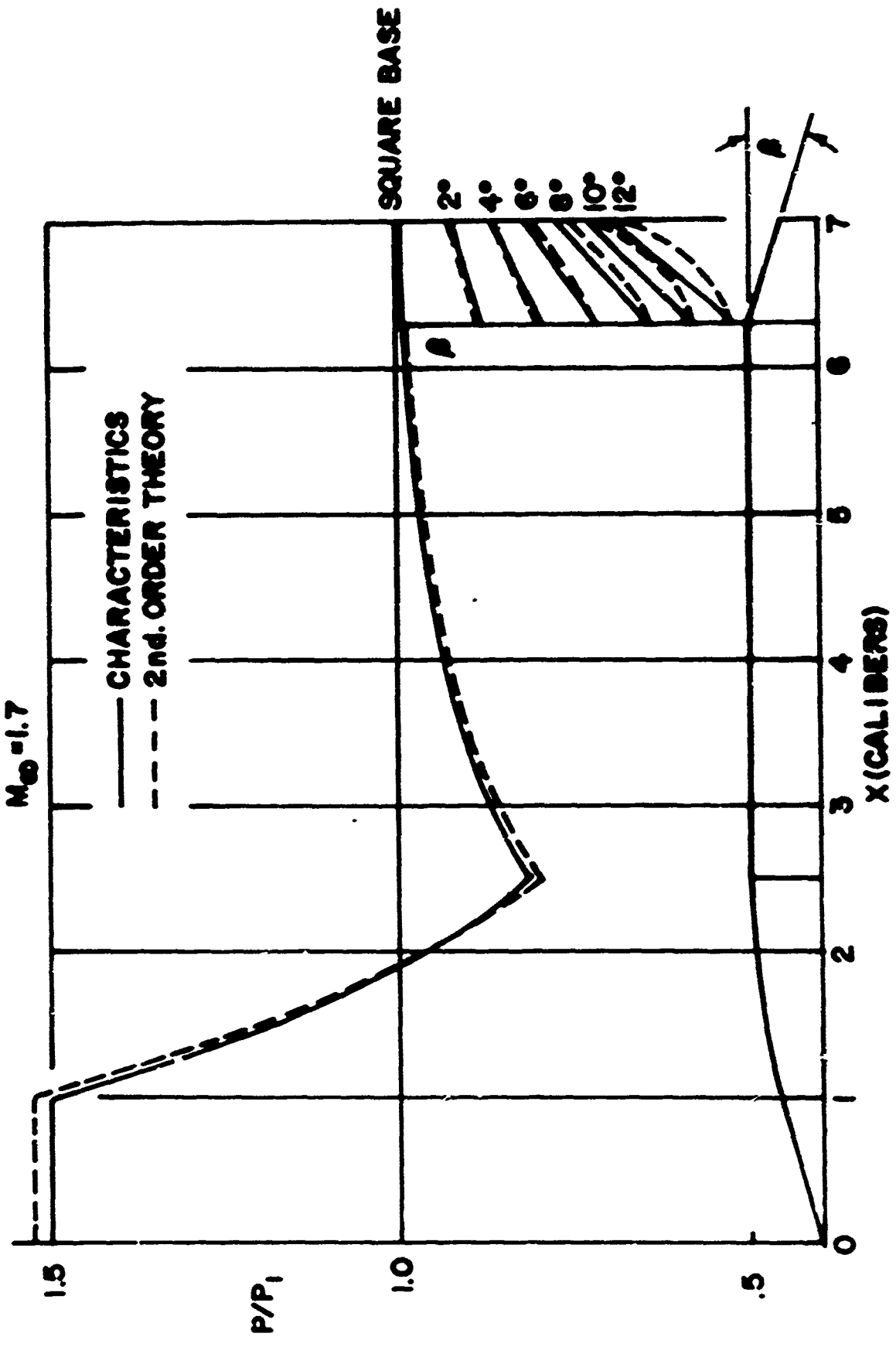


FIG. 5 PRESSURE RATIO ALONG A BOATTAINED PROJECTILE

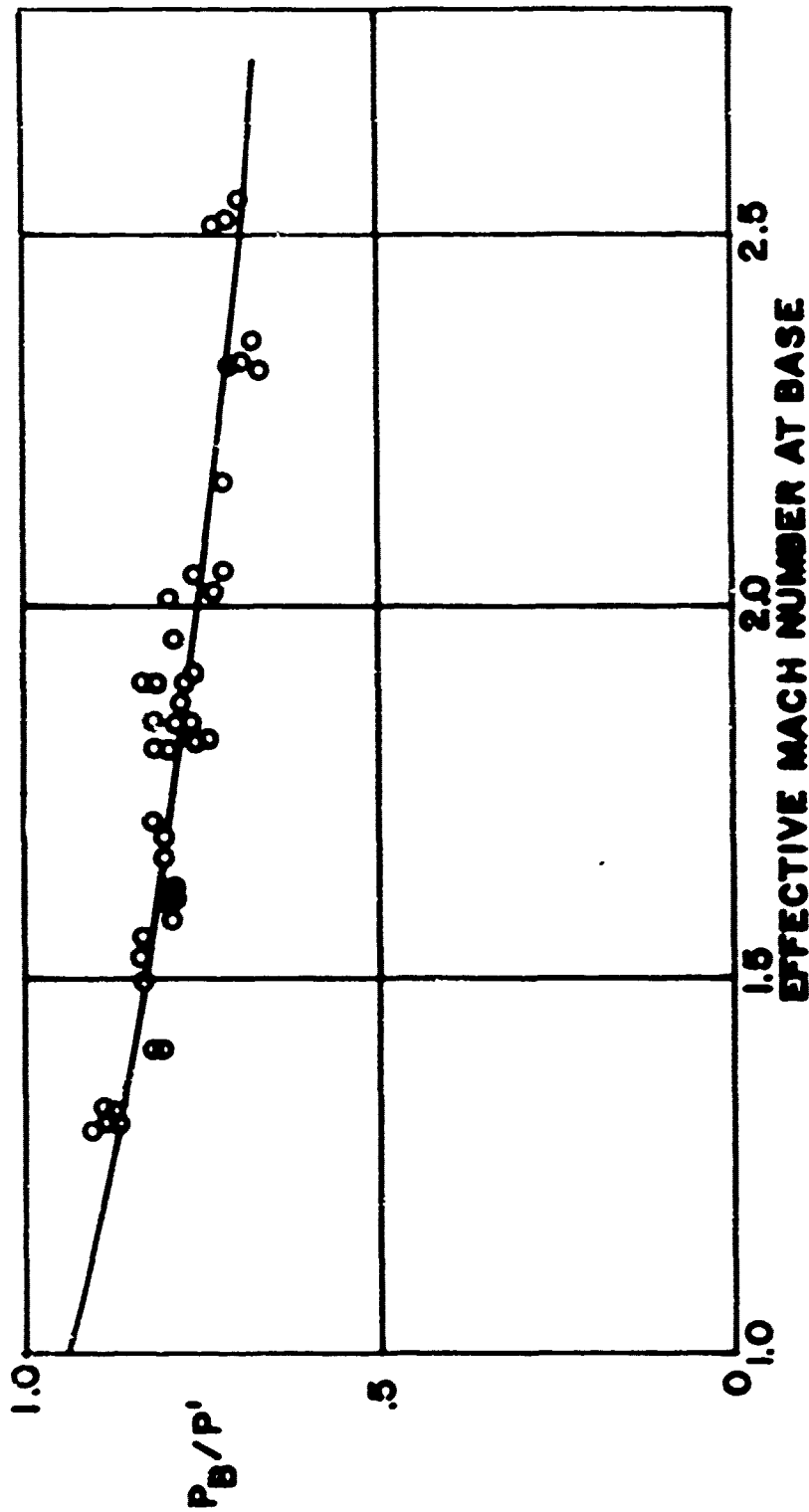


FIG.6 RATIO OF BASE PRESSURE TO LOCAL STATIC PRESSURE
 vs
 MACH NUMBER

- BRL RANGE
- PRESENT THEORY
- - - POTENTIAL THEORY

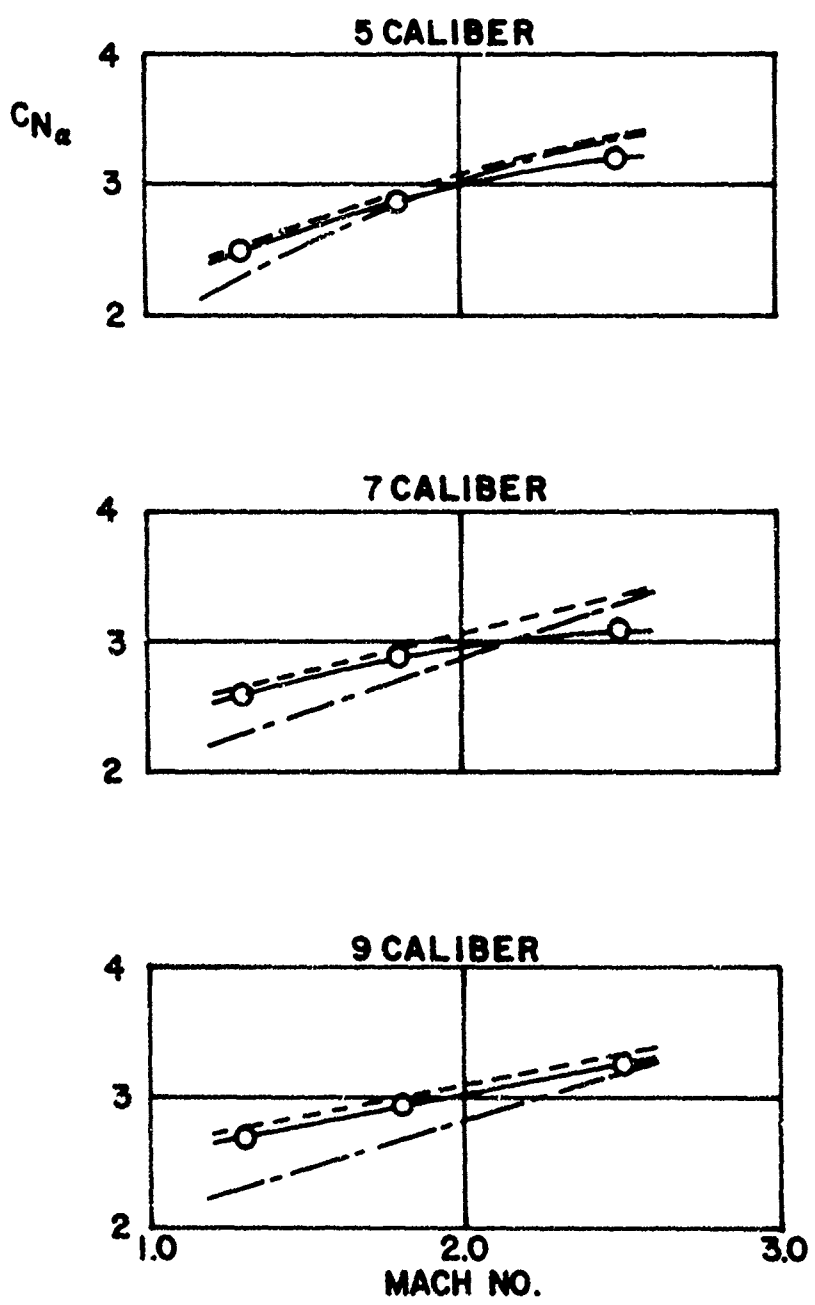
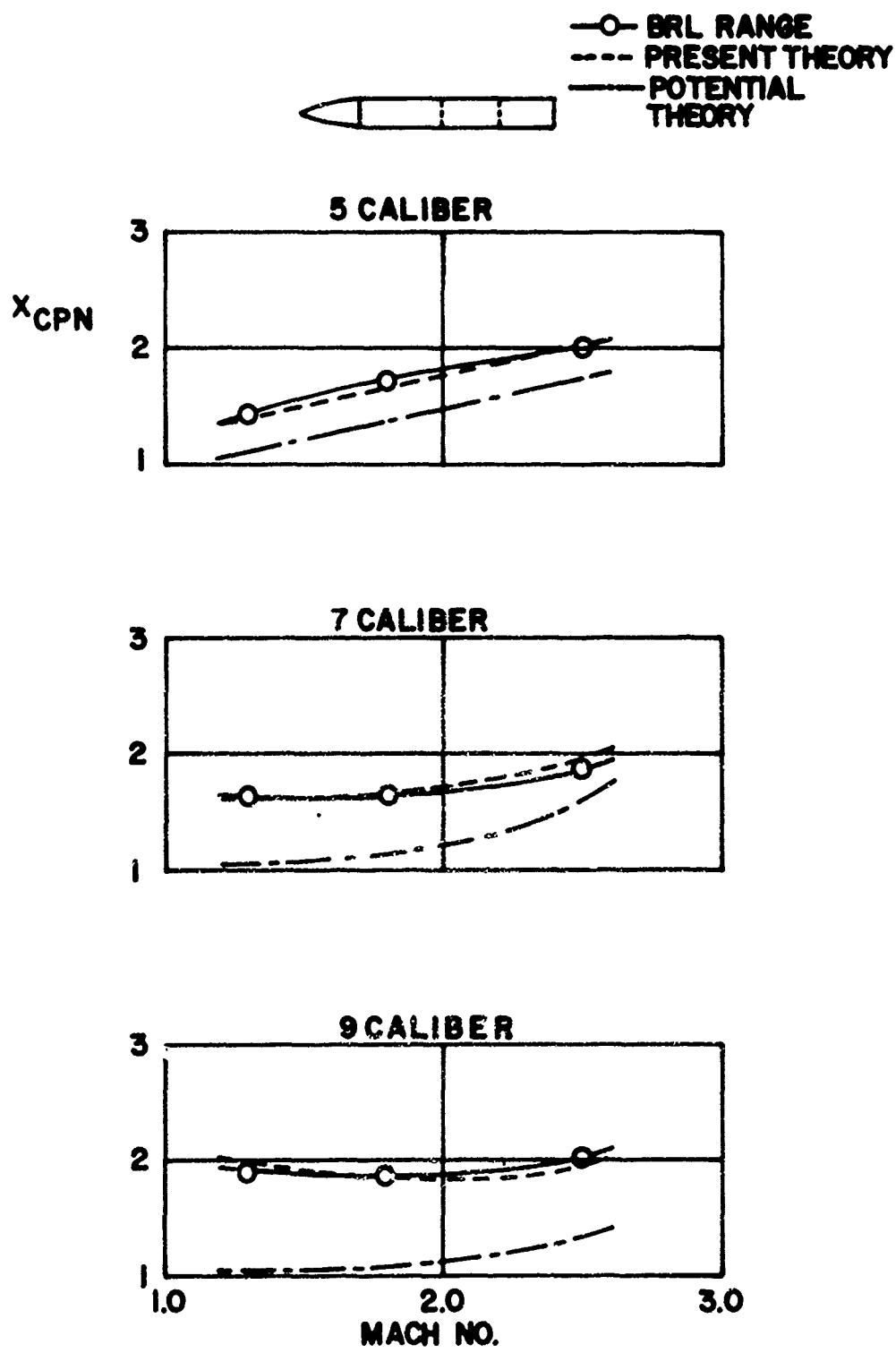


FIG.7 NORMAL FORCE SLOPE
vs
MACH NUMBER



**FIG. 8 NORMAL FORCE CENTER OF PRESSURE
VS
MACH NUMBER**

○ BRL RANGE
 --- PRESENT THEORY

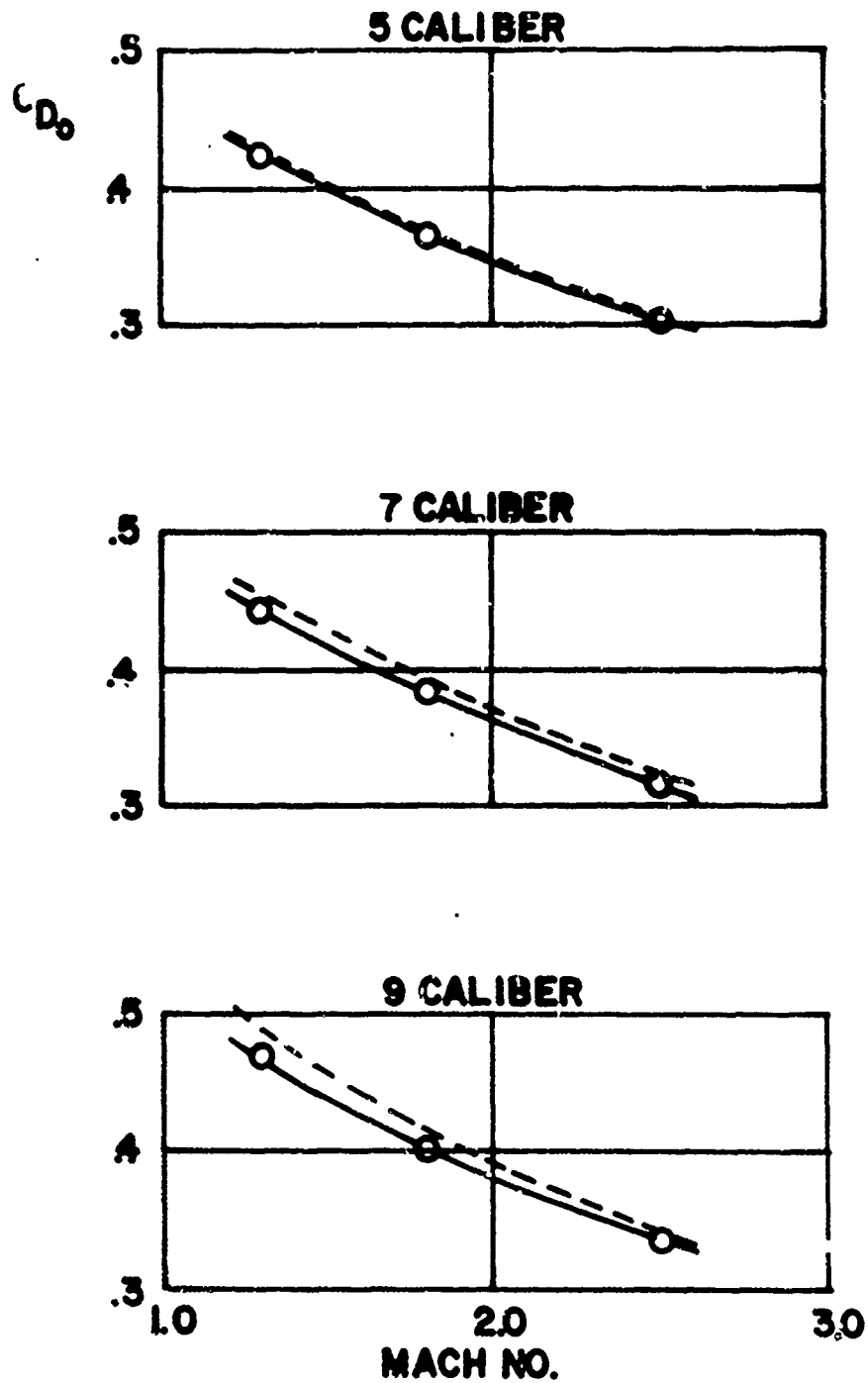
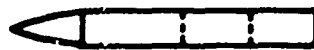
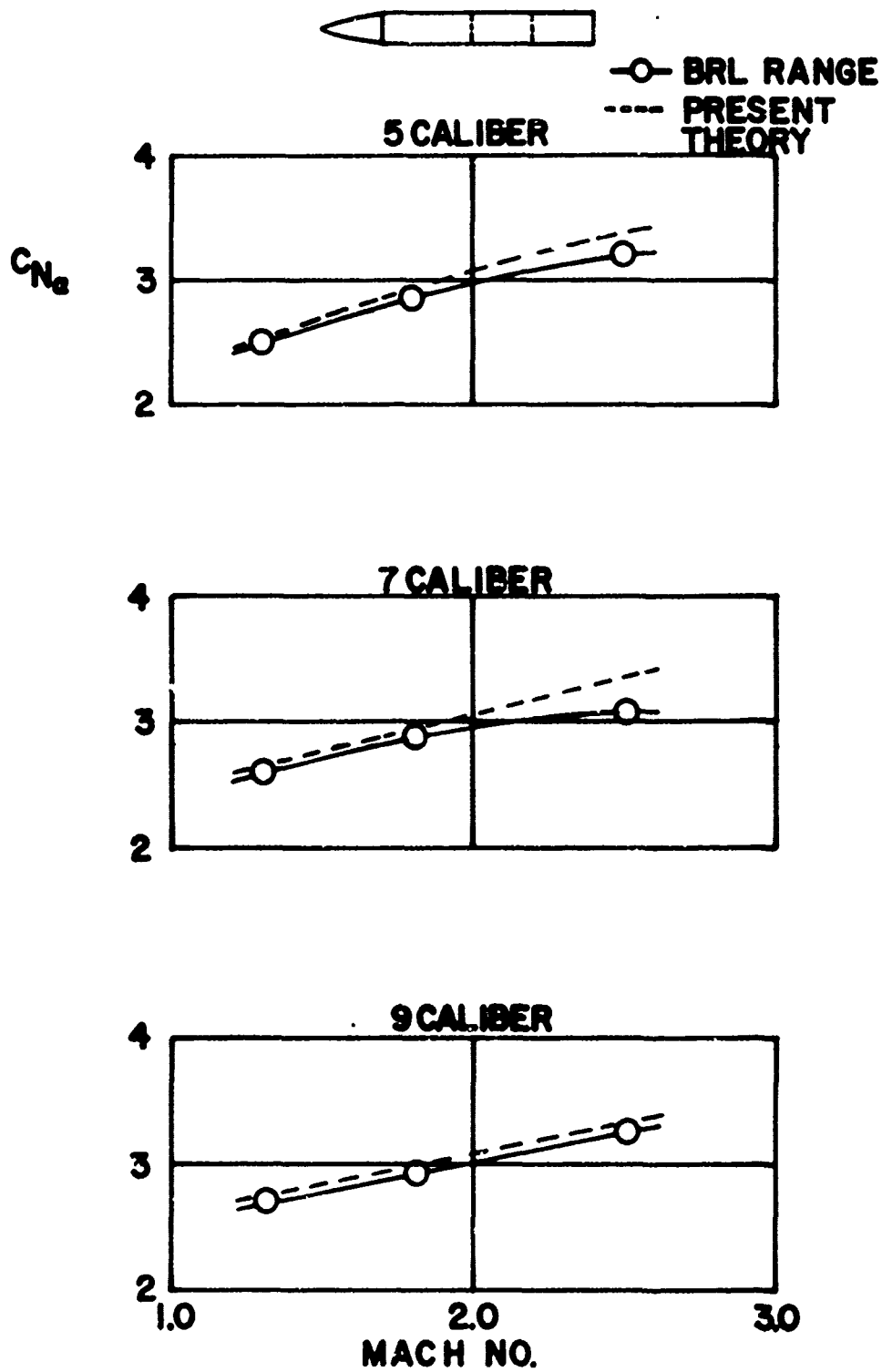
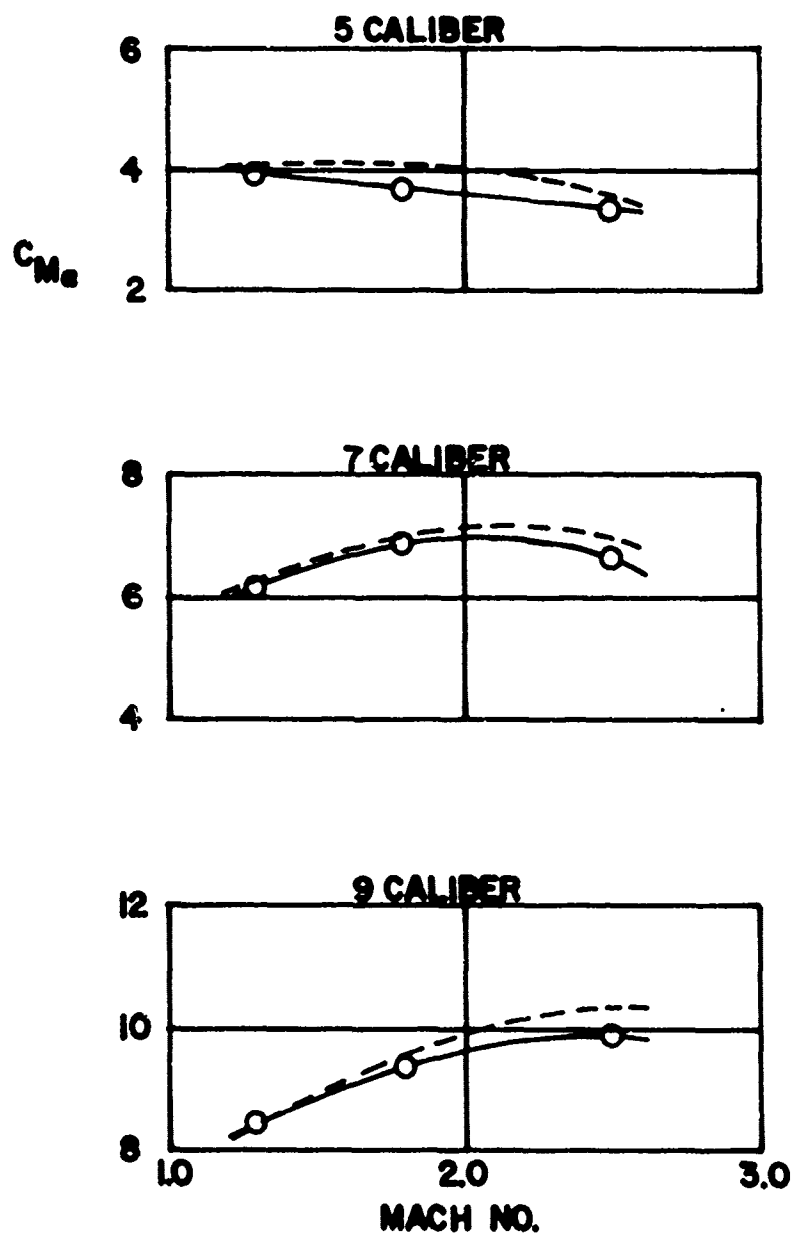


FIG.9 ZERO-YAW DRAG COEFFICIENT
 VS
 MACH NUMBER



**FIG. 10 NORMAL FORCE COEFFICIENT
VS
MACH NUMBER**

○ BRL RANGE
 --- PRESENT THEORY



**FIG. II STATIC MOMENT COEFFICIENT
 VS
 MACH NUMBER**

○ BRL RANGE
 --- PRESENT THEORY

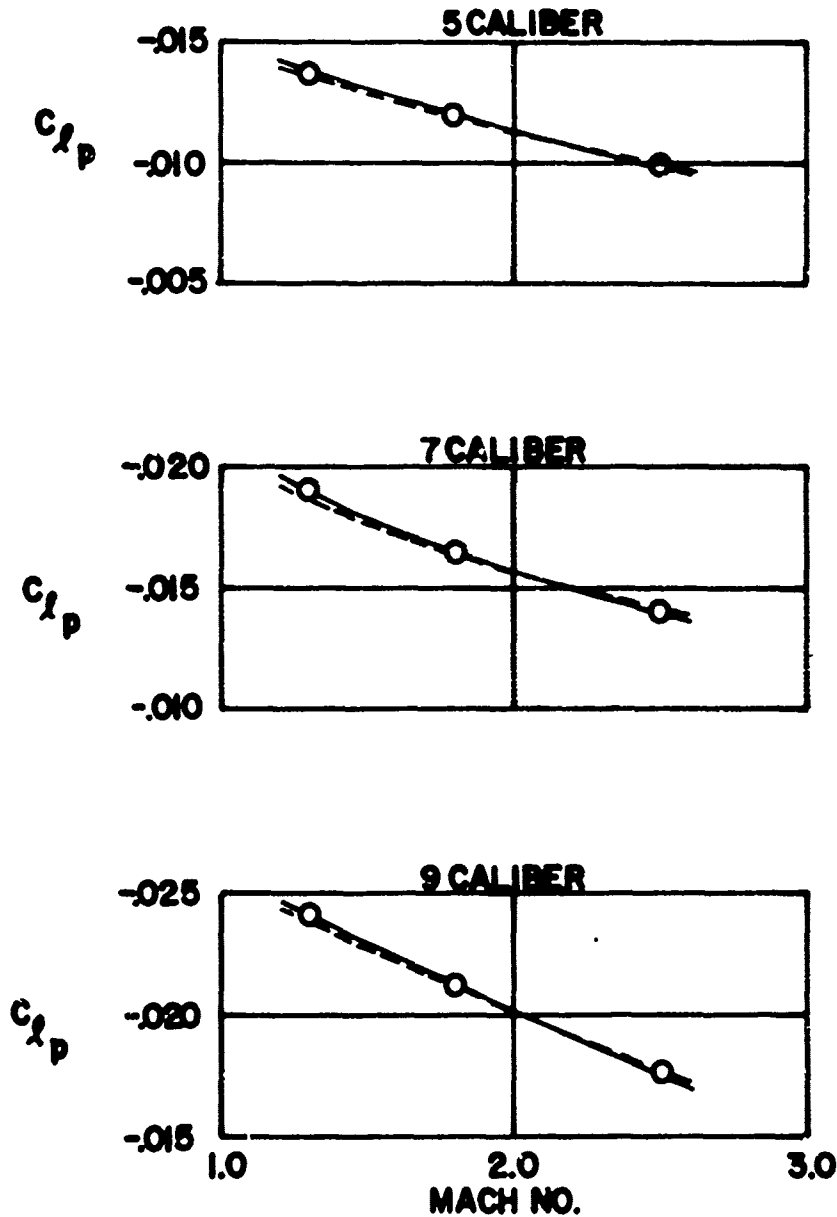
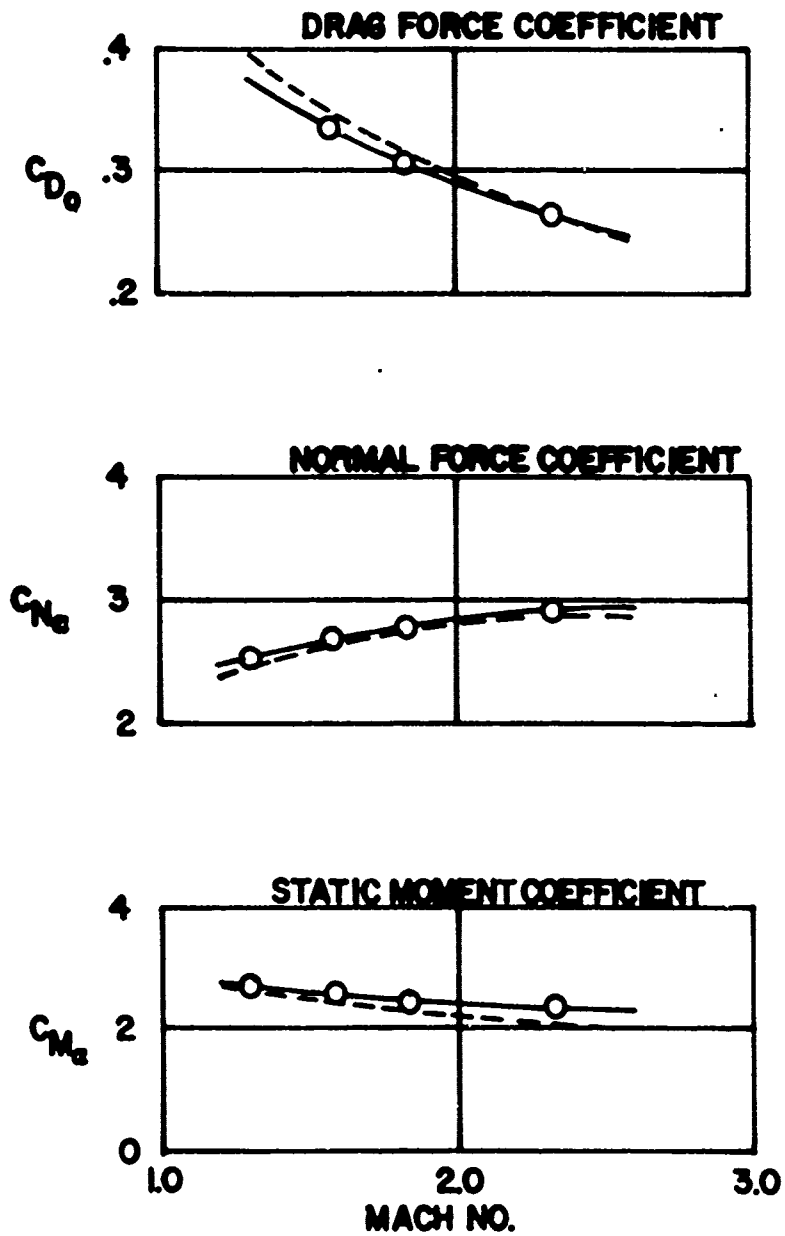


FIG. 12 ROLL DAMPING MOMENT COEFFICIENT
 vs
 MACH NUMBER

-○- BRL RANGE
 --- PRESENT THEORY



**FIG. 13 DRAG, NORMAL FORCE, AND
 STATIC MOMENT COEFFICIENTS
 VS
 MACH NUMBER**

○ BRL RANGE
 --- PRESENT THEORY

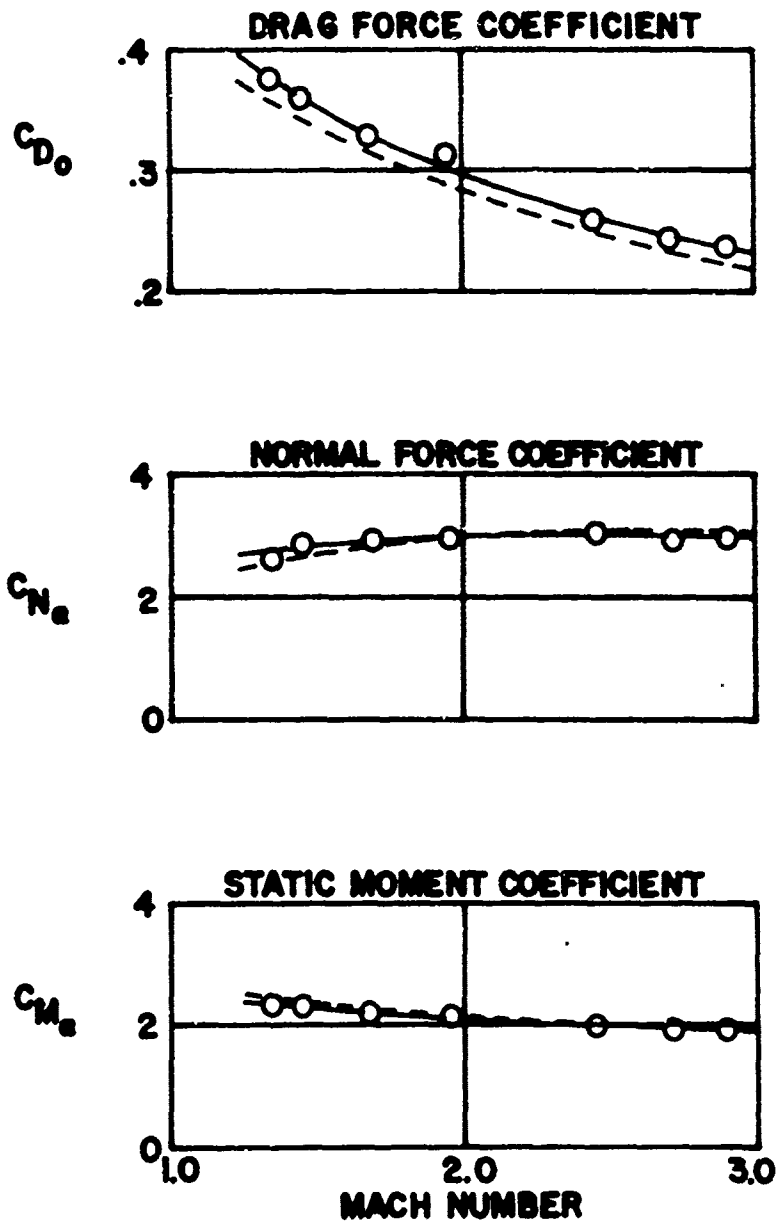


FIG. 14 DRAG, NORMAL FORCE AND STATIC MOMENT COEFFICIENTS vs MACH NUMBER



$M_\infty = 1.7$

—○— BRL RANGE
 - - - PRESENT THEORY

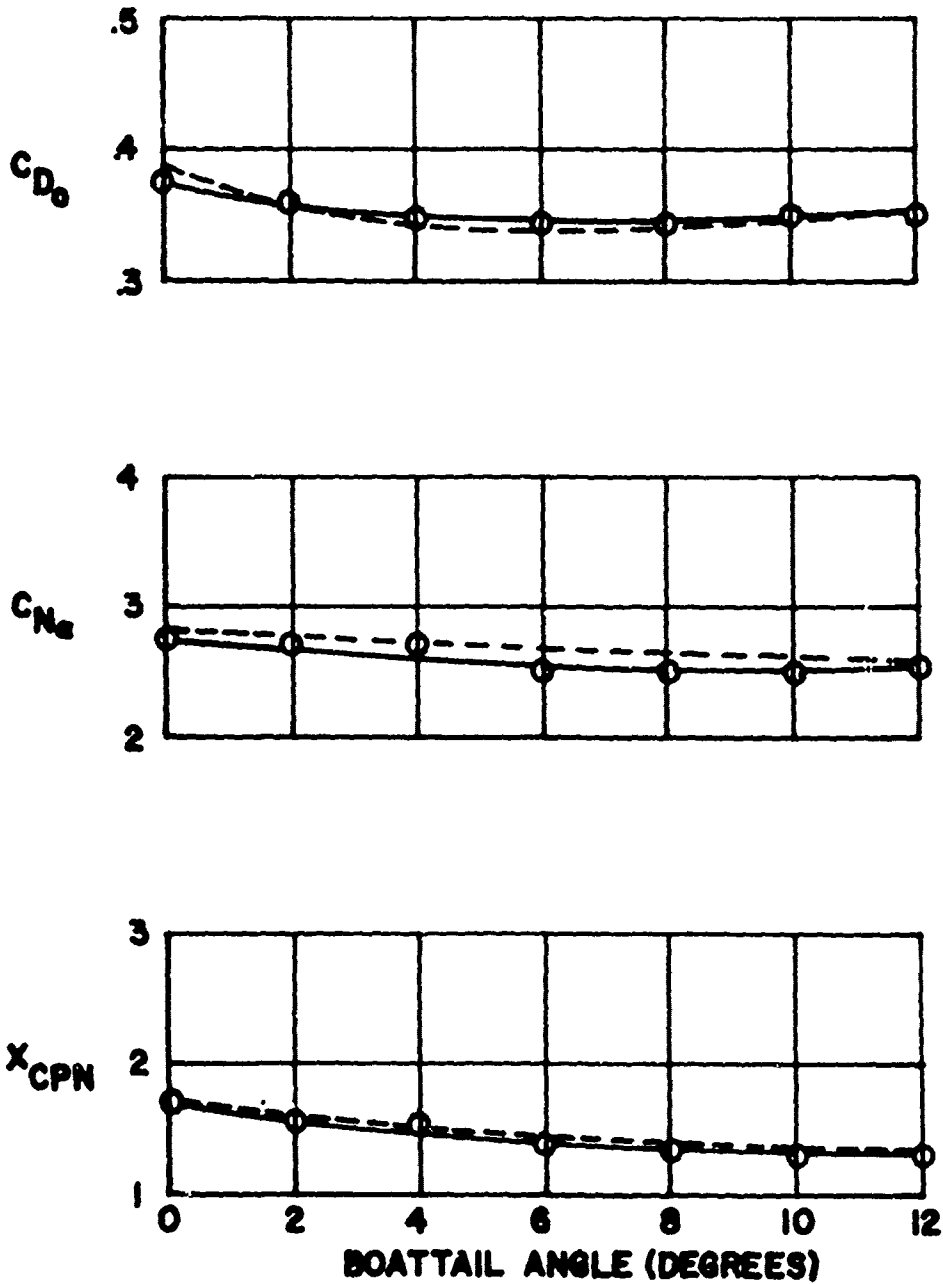


FIG.15 DRAG, NORMAL FORCE, AND CENTER OF PRESSURE vs BOATTAIL ANGLE

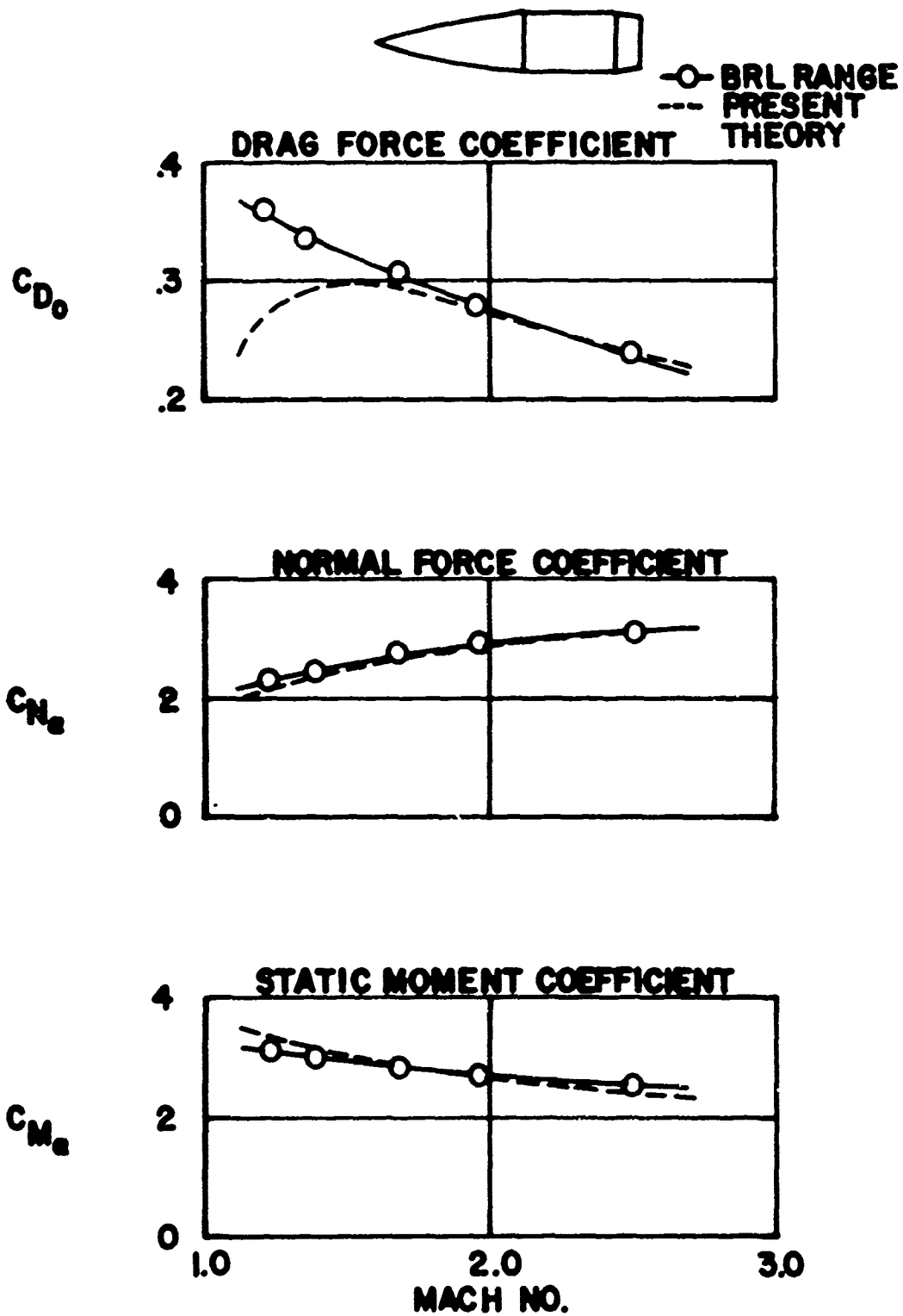


FIG. 16 DRAG, NORMAL FORCE AND STATIC MOMENT COEFFICIENTS vs MACH NUMBER

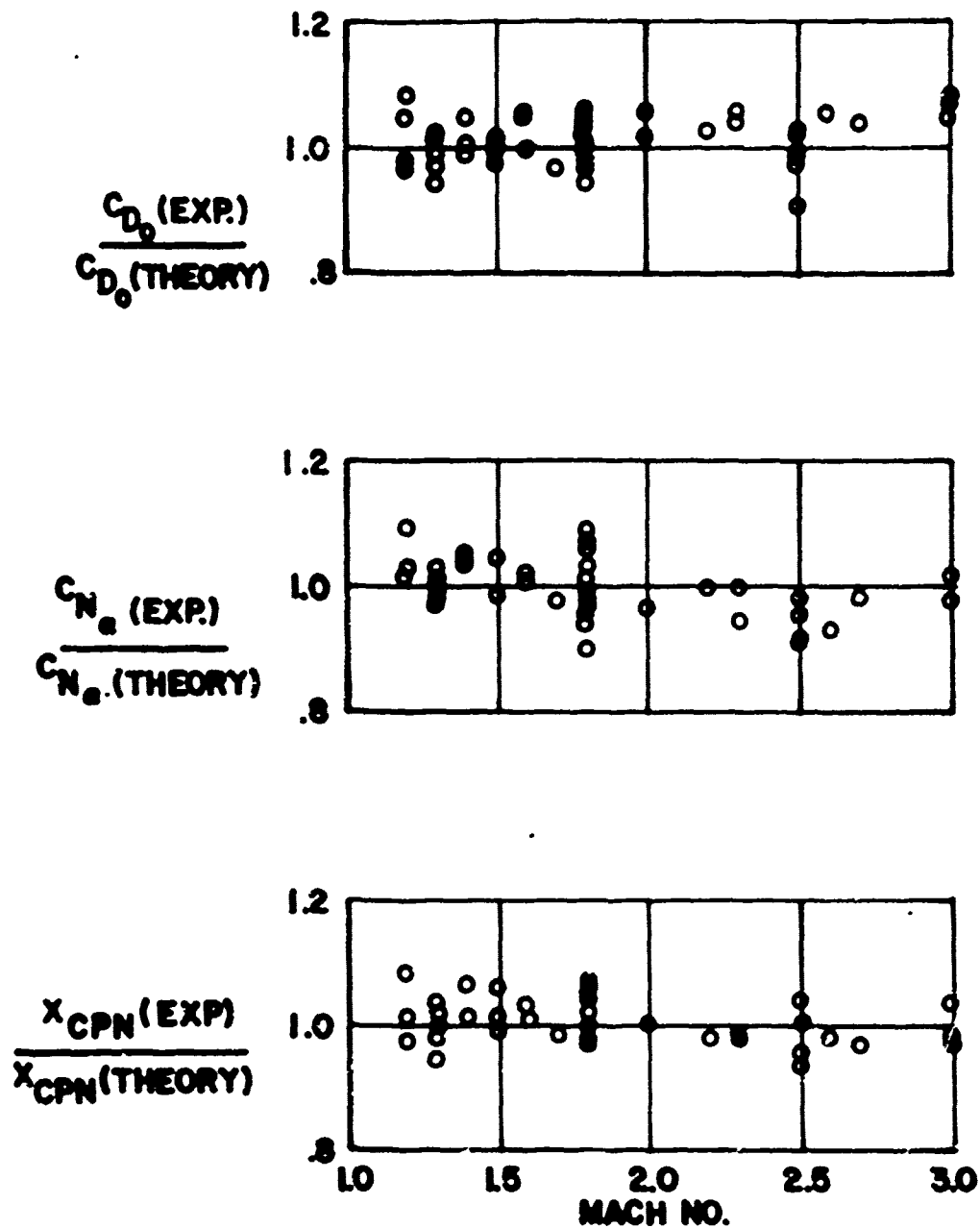


FIG. 17 RATIO OF EXPERIMENTAL TO THEORETICAL DRAG, NORMAL FORCE AND CENTER OF PRESSURE FOR SQUARE BASED MODELS

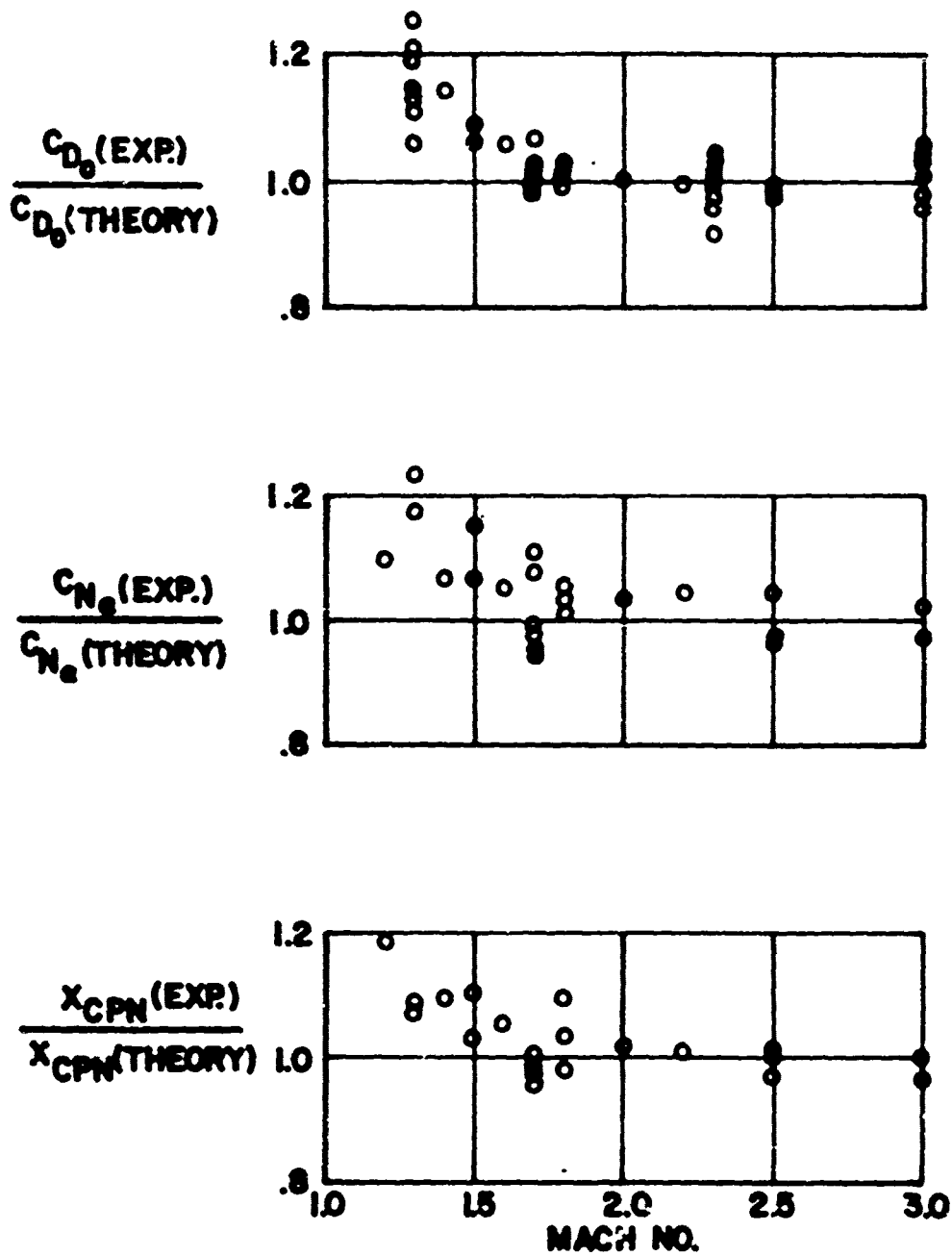


FIG. 18 RATIO OF EXPERIMENTAL TO THEORETICAL DRAG, NORMAL FORCE, AND CENTER OF PRESSURE FOR BOATTAILED MODELS

REFERENCES

1. H. P. Hitchcock, "On Estimating the Drag Coefficient of Missiles," Ballistic Research Laboratories Memorandum Report 545, AD 802065, May 1951.
2. N. Simmons, "Simplified Methods of Estimating Static Stability of Air and Underwater Projectiles," Fort Halstead: ADE TR-14/52, or Project Note 21, 1952.
3. R. M. Wood, "Quick Methods for Estimating the Static Aerodynamic Coefficients of Shell," Ballistic Research Laboratories Memorandum Report 854, AD 59599, November 1954.
4. R. M. Wood and C. H. Murphy, "Aerodynamic Derivatives for Both Steady and Non-Steady Motion of Slender Bodies," Ballistic Research Laboratories Memorandum Report 880, AD 66178, April 1955.
5. R. H. Whyte, "Spinner" - A Computer Program for Predicting the Aerodynamic Coefficients of Spin Stabilized Projectiles, General Electric Technical Report TIS69APB3, 1969.
6. M. D. Van Dyke, First and Second Order Theory of Supersonic Flow Past Bodies of Revolution, Journal of Aeronautical Sciences, March 1951.
7. M. D. Van Dyke, "Practical Calculation of Second-Order Supersonic Flow Past Nonlifting Bodies of Revolution," NACA Technical Note 2744, 1952.
8. E. R. Van Driest, Turbulent Boundary Layers in Compressible Fluids, Journal of Aeronautical Sciences, March 1951.
9. D. R. Chapman, "An Analysis of Base Pressure at Supersonic Velocites and Comparison with Experiment," NACA Report 1051, 1951.
10. J. Sternberg, Effect of a Boattail on the Base Pressure, Memorandum to R. H. Kent, May 1948 (Reproduced in Ballistic Research Laboratories Report 1295; see Reference 16).
11. A. C. Charters and R. H. Kent, "The Relation Between the Skin Friction Drag and the Spin Reducing Torque," Ballistic Research Laboratories Report 187, AD 491854, July 1942.

17. A. C. Charters and R. A. Turetsky, "Determination of Base Pressure From Free-Flight Data," Ballistic Research Laboratories Report 653, ATI 26679L, March 1948.
13. R. A. Turetsky, "Cone Cylinder Model E12M3," Ballistic Research Laboratories Memorandum Report 435, AD 492775, July 1946.
14. L. E. Schmidt, "The Dynamic Properties of Pure Cones and Cone Cylinders," Ballistic Research Laboratories Memorandum Report 759, AD 30249, January 1954.
15. C. H. Murphy and L. E. Schmidt, "The Effect of Length on the Aerodynamic Characteristics of Bodies of Revolution in Supersonic Flight," Ballistic Research Laboratories Report 867, AD 23468, August 1953.
16. B. G. Karpov, "The Effect of Various Boattail Shapes on Base Pressure and Other Aerodynamic Characteristics of a 7-Caliber Long Body of Revolution at $M=1.70$," Ballistic Research Laboratories Report 1295, AD 474352, August 1965.
17. E. R. Dickinson, "Some Aerodynamic Effects of Varying the Body Length and Head Length of a Spinning Projectile," Ballistic Research Laboratories Memorandum Report 1664, AD 469897, July 1965.
18. E. D. Boyer, "Free Flight Range Tests of a 10-Caliber Cone Cylinder," Ballistic Research Laboratories Memorandum Report 1258, AD 237579, April 1960.
19. E. R. Dickinson, "The Effect of Boattailing on the Drag Coefficient of Cone-Cylinder Projectiles at Supersonic Velocities," Ballistic Research Laboratories Memorandum Report 842, AD 57769, November 1954.
20. G. L. Winchenbach, R. M. Watt and A. G. Skinner, "Free Flight Range Tests of Basic and Boattail Configurations of 3- and 5-Caliber Army-Navy Spinner Projectiles," AEDC Technical Report 70-12, AD 866458, March 1970.
21. E. R. Dickinson, "The Effects of Annular Rings and Grooves, and of Body Undercuts on the Aerodynamic Properties of a Cone-Cylinder Projectile at $M=1.72$," Ballistic Research Laboratories Memorandum Report 1284, AD 242497, June 1960.

22. W. E. Scott, "The Effect of a Rotating Band Upon Some Aerodynamic Coefficients of the Seven-Caliber Army-Navy Spinner Rocket at Mach 1.8," Ballistic Research Laboratories Memorandum Report 1302, AD 246223, September 1960.
23. T. J. Mueller and C. R. Hall, "Analytical Prediction of the Turbulent Base Pressure in Supersonic Axisymmetric Flow Including the Effect of Initial Flow Direction," AFFDL-TR-68-132, September 1968.
24. R. H. Page, "Annual Report - Separated Flows, 1969 to 1970," AFOSR 70-2514TR, 1970.
25. A. L. Addy, "Analysis of the Axisymmetric Base Pressure and Base Temperature Problem with Supersonic Interacting Free-Stream Nozzle Flows Based on the Flow Model of Korst, et, Part III," U. S. Army Missile Command Report No. RD-TR-69-14, February 1970.
26. F. G. Moore, "Body Alone Aerodynamics of Guided and Unguided Projectiles at Subsonic, Transonic, and Supersonic Mach Numbers," Naval Weapons Laboratory Technical Report TR-2796, AD 754098, November 1972.

APPENDIX

The Van Dyke Hybrid Theory.

The theory described in this appendix is essentially that given by Van Dyke in References 6 and 7, and is restated here for completeness.

For a body of revolution at an angle of attack, α , in a uniform supersonic stream, the boundary condition at the body surface is simplified by choosing a cylindrical coordinate system in body axes. The free stream velocity, U , is resolved into axial and cross-flow components, as in Figure A-1.

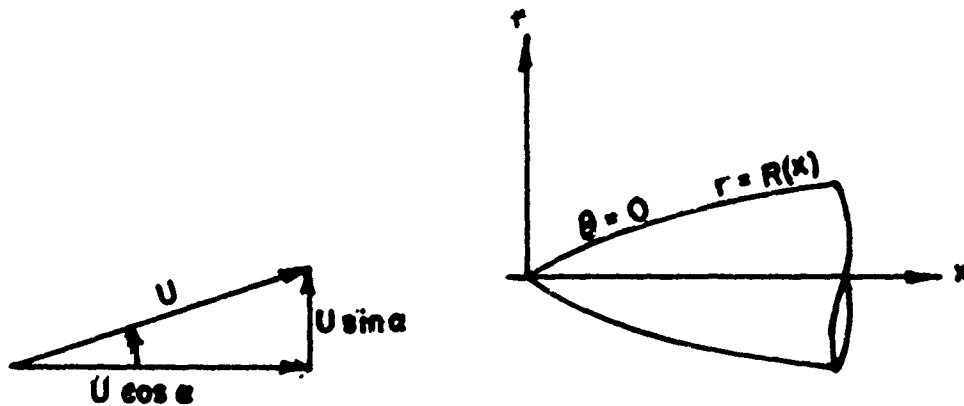


Figure A-1. Cylindrical Coordinate System in Body Axes

The equation of motion in terms of the velocity potential $\phi_0(x, r, \theta)$ is;

$$\begin{aligned}
 & (c^2 - \Omega_x^2) \Omega_{xx} + (c^2 - \Omega_r^2) \Omega_{rr} + (c^2 - \Omega_\theta^2/r^2) (\Omega_{\theta\theta}/r^2) \\
 & + (c^2 + \Omega_\theta^2/r^2) (\Omega_r/r) - 2 \Omega_r \Omega_\theta \Omega_{r\theta}/r^2 - 2 \Omega_\theta \Omega_x \Omega_{\theta x}/r^2
 \end{aligned} \tag{A.1}$$

$$- 2 \Omega_x \Omega_r \Omega_{xr} = 0$$

The speed of sound, c , is related to c_0 , its free stream value, by;

$$c^2 = c_0^2 - \frac{1}{2}(\gamma-1) [\zeta_x^2 + \zeta_r^2 + \zeta_\theta^2/r^2 - U^2] \quad (\text{A. 2})$$

Subscripts indicate partial differentiation.

The perturbation potential $\zeta(x, r, \theta)$ is defined as;

$$\zeta(x, r, \theta) = U [x \cos \alpha + r \sin \alpha \cos \theta + \zeta(x, r, \theta)]. \quad (\text{A. 3})$$

The axial, radial, and azimuthal velocity components are given by;

$$\begin{aligned} u/U &= \zeta_x/U = \cos \alpha + \zeta_x \\ v/U &= \zeta_r/U = \sin \alpha \cos \theta + \zeta_r \\ w/U &= \zeta_\theta/rU = -\sin \alpha \sin \theta + \zeta_\theta/r \end{aligned} \quad (\text{A. 4})$$

The free stream Mach number, M , is defined as;

$$M = U/c_0. \quad (\text{A. 5})$$

Substitution of equations (A. 2), (A. 3), and (A. 5) into (A. 1) gives the equation of motion in terms of the perturbation potential,

$$\begin{aligned}
\psi_{rr} + \psi_r/r + \psi_{\theta\theta}/r^2 - \beta^2 \psi_{xx} = M^2 \left\{ \frac{1}{2} (\gamma-1) (\psi_{xx} + \psi_{rr} + \psi_r/r + \right. \\
\psi_{\theta\theta}/r^2) [2 (\psi_x \cos \alpha + \psi_r \sin \alpha \cos \theta - \psi_\theta \sin \alpha \sin \theta/r) + \\
\psi_x^2 + \psi_r^2 + \psi_\theta^2/r^2] + \psi_{xx} (2 \psi_x \cos \alpha + \psi_x^2 - \sin^2 \alpha) + \\
\psi_{rr} (\psi_r + \sin \alpha \cos \theta)^2 + (\psi_{\theta\theta}/r^2 - \psi_r/r) (\psi_\theta/r - \sin \alpha \sin \theta)^2 + \\
2 \psi_{xr} (\psi_x + \cos \alpha) (\psi_r + \sin \alpha \cos \theta) + 2 (\psi_{x\theta}/r) (\psi_x + \cos \alpha) (\psi_\theta/r - \\
\sin \alpha \sin \theta) + 2 (\psi_{r\theta}/r) (\psi_r + \sin \alpha \cos \theta) (\psi_\theta/r - \sin \alpha \sin \theta) - \\
\left. 2 \sin \alpha (\psi_\theta/r - \sin \alpha \sin \theta) (\psi_r \sin \theta/r + \psi_\theta \cos \theta/r^2) \right\}, \quad (A. 6)
\end{aligned}$$

where $\beta^2 = M^2 - 1$.

Since the incident stream is supersonic, all perturbations must vanish upstream of the body, and the condition of tangent flow must be imposed on the body surface. The appropriate boundary conditions are,

$$\psi(0, r, \theta) = \psi_x(0, r, \theta) = 0. \quad (A. 7)$$

$$\psi_r(x, R, \theta) + \sin \alpha \cos \theta = R' [\cos \alpha + \psi_x(x, R, \theta)], \quad (A. 8)$$

where $R = R(x)$, the local body radius, and $R' = \frac{dR}{dx}$, the local body slope.

Although the exact nonlinear equations (A. 6), (A. 7), and (A. 8) could be formally attacked by finite difference methods, a satisfactory approximation to the solution is more easily obtained by an iterative technique, based on a first order solution, which assumes that the entire right hand side of (A. 6) can be neglected. The first order potential is denoted by φ , and the first order problem is given by,

$$\varphi_{rr} + \varphi_r/r + \varphi_{\theta\theta}/r^2 - \beta^2 \varphi_{xx} = 0. \quad (\text{A. 9})$$

$$\varphi(0, r, \theta) = \varphi_x(0, r, \theta) = 0. \quad (\text{A. 10})$$

$$\varphi_r(x, R, \theta) + \sin \alpha \cos \theta = R' [\cos \alpha + \varphi_x(x, R, \theta)]. \quad (\text{A. 11})$$

The first order problem can be further simplified by splitting the axial and cross-flow components into two independent problems.

$$\text{Let } \varphi(x, r, \theta) = \varphi_0(x, r) \cos \alpha + \varphi_1(x, r) \sin \alpha \cos \theta \quad (\text{A. 12})$$

where φ_0 is the potential of axial flow, and φ_1 is the potential of the cross-flow. Substitution of (A. 12) into (A. 9), (A. 10), and (A. 11) gives, for the axial flow,

$$\varphi_{0rr} + \varphi_{0r}/r - \beta^2 \varphi_{0xx} = 0 \quad (\text{A. 13})$$

$$\varphi_0(0, r) = \varphi_{0x}(0, r) = 0 \quad (\text{A. 14})$$

$$\varphi_{0r}(x, R) = R' [1 + \varphi_{0x}(x, R)] \quad (\text{A. 15})$$

and for the cross flow,

$$\varphi_{1rr} + \varphi_{1r}/r - \varphi_{1r}/r^2 - \beta^2 \varphi_{1xx} = 0 \quad (\text{A. 16})$$

$$\varphi_1(0, r) = \varphi_{1x}(0, r) = 0 \quad (\text{A. 17})$$

$$1 + \varphi_{1r}(x, R) = R' \varphi_{1x}(x, R). \quad (\text{A. 18})$$

The general solution of (A. 13) and (A. 16), which satisfy the appropriate boundary conditions are,

$$\varphi_0(x, r) = - \int_0^{x-\beta r} \frac{f(\xi) d\xi}{\sqrt{(x-\xi)^2 - \beta^2 r^2}} \quad (\text{A. 19})$$

$$\varphi_1(x, r) = \frac{1}{\beta r} \int_0^{x-\beta r} \frac{(x-\xi) g(\xi) d\xi}{\sqrt{(x-\xi)^2 - \beta^2 r^2}} \quad (\text{A. 20})$$

The unknown function $f(\xi)$ appearing in equation (A. 19) represents a distribution of sources and sinks along the x -axis, and $g(\xi)$ in equation (A. 20) represents an axial distribution of doublets. The functions $f(\xi)$ and $g(\xi)$ are determined by satisfying the tangency conditions, equations (A. 15) and (A. 18), along the body surface.

If the first order solution (A. 12) is now substituted in the right hand side of (A. 6), a second order iteration equation results. The complete second order potential, ϕ , can also be split into axial and cross-flow components,

$$\phi(x, r, \theta) = \phi_0 \cos \alpha + \phi_1 \sin \alpha \cos \theta + \dots \quad (\text{A. 21})$$

Substituting equations (A. 12) and (A. 21) into (A. 6), and noting that φ_0 and φ_1 satisfy equations (A. 13) and (A. 16), respectively, the second order iteration equations become, for the axial flow,

$$\begin{aligned}
\varphi_{0_{rr}} + \varphi_{0_r}/r - \beta^2 \varphi_{0_{xx}} &= M^2 \{ 2 \varphi_{0_{xr}} \varphi_{0_r} + [2 + (\gamma-1)M^2] \varphi_{0_{xx}} \varphi_{0_x} + \\
\varphi_{0_{rr}} \varphi_{0_r}^2 + \frac{1}{2} (\gamma-1) M^2 \varphi_{0_{xx}} \varphi_{0_r}^2 + 2 \varphi_{0_{xr}} \varphi_{0_x} \varphi_{0_r} + & \quad (A.22) \\
[1 + \frac{1}{2} (\gamma-1) M^2] \varphi_{0_{xx}} \varphi_{0_x}^2 \} &
\end{aligned}$$

and for the cross-flow,

$$\begin{aligned}
\varphi_{1_{rr}} + \varphi_{1_r}/r - \varphi_{1_r}/r^2 - \beta^2 \varphi_{1_{xx}} &= M^2 \{ 2 \varphi_{0_{xr}} (1 - \varphi_{0_x})(1 + \varphi_{1_r}) + \\
2 \varphi_{0_{rr}} \varphi_{0_r} (1 + \varphi_{1_r}) + 2 \varphi_{0_r} (1 + \varphi_{0_x}) \varphi_{1_{xr}} + \varphi_{0_r}^2 \varphi_{1_{rr}} + & \\
\frac{1}{2} (\gamma-1) M^2 \varphi_{1_{xx}} (2 \varphi_{0_x} + \varphi_{0_x}^2 + \varphi_{0_r}^2) + \varphi_{0_x} (2 + \varphi_{0_x}) \varphi_{1_{xx}} + & \quad (A.23) \\
(\gamma-1) M^2 \varphi_{0_{xx}} [(1 + \varphi_{0_x}) \varphi_{1_x} + \varphi_{0_r} (1 + \varphi_{1_r})] + 2 \varphi_{0_{xx}} (1 + \varphi_{0_x}) \varphi_{1_x} + & \\
2 \varphi_{0_{xr}} \varphi_{0_r} \varphi_{1_x} \} &
\end{aligned}$$

Both equations (A. 22) and (A. 23) can be simplified somewhat by consideration of the order of magnitude estimates on inhomogeneous terms. In equation (A. 22), at moderate supersonic speeds, the first three terms on the right hand side contribute to φ_{0_x} quantities of order $\epsilon^4 \log^2 \epsilon$, $\epsilon^4 \log \epsilon$, and ϵ^4 , where ϵ is the body thickness ratio. The last three terms in equation (A. 22) contributed, at most, quantities of order $\epsilon^6 \log^3 \epsilon$. Near the hypersonic limit, the first

four inhomogeneous terms contribute $O[\epsilon^2]$, and the last two, $O[\epsilon^4]$. For either speed regime, the last two terms in (A. 22) may be neglected in comparison with the first four inhomogeneous terms.

In equation (A. 23), inhomogeneous terms may be neglected if they contribute to ϕ_{1x} no more than $O[\epsilon^5 \log \epsilon]$ at moderate supersonic speeds, and $O[\epsilon^3]$ at hypersonic speeds. Neglecting the appropriate terms, equations (A. 22) and (A. 23) simplify to,

$$\begin{aligned} \phi_{0rr} + \phi_{0r}/r - \beta^2 \phi_{0xx} = M^2 \{ 2\phi_{0r} \phi_{0xr} + [2 + (\gamma-1)M^2] \phi_{0x} \phi_{0xx} + \\ \phi_{0r}^2 \phi_{0rr} + [\frac{1}{2}(\gamma-1)] M^2 \phi_{0r}^2 \phi_{0xx} \}. \end{aligned} \quad (\text{A. 24})$$

$$\begin{aligned} \phi_{1rr} + \phi_{1r}/r + \phi_{1r}/r^2 - \beta^2 \phi_{1xx} = 2M^2 \left[\phi_{0xr} (1 + \phi_{1r}) + \phi_{0r} \phi_{1xr} + \right. \\ \left. \phi_{0rr} \phi_{0r} (1 + \phi_{1r}) + \frac{1}{2} \phi_{0r}^2 \phi_{1rr} + \frac{1}{2} (\gamma-1) M^2 \{ \phi_{0xx} [\phi_{1x} + \phi_{0r} (1 + \phi_{1r})] + \right. \\ \left. \phi_{1xx} (\phi_{0x} + \frac{1}{2} \phi_{0r}^2) \} + \phi_{0xx} \phi_{1x} + \phi_{0x} \phi_{1xx} + \phi_{0xr} \phi_{0x} \right]. \end{aligned} \quad (\text{A. 25})$$

The inhomogeneous wave equations (A. 24) and (A. 25) could be attacked by standard numerical methods; however, if any particular solution of these equations were known, the boundary condition could be corrected by adding solutions of the homogeneous equations (A. 13) and (A. 16), and the second order problem would be reduced to an equivalent first order problem.

Van Dyke discovered an approximate particular solution, denoted by Ψ_0 , to equation (A. 24), stated in terms of the first order potential and its first derivatives,

$$\Psi_0 = M^2 \left\{ \varphi_{0x} \left[\varphi_0 + \frac{1}{2} (\gamma+1) (M^2/\beta^2) r \varphi_{0r} \right] - \frac{1}{4} r \varphi_{0r}^3 \right\}. \quad (\text{A. 25})$$

This particular solution satisfies the iteration equation within the order of terms already neglected, at moderate supersonic speeds. Van Dyke states^[6] that although it fails to account completely for triple products at hypersonic speeds, numerical examples have shown the actual magnitude of error to be small.

A particular solution of the iteration equation for the cross-flow (A. 25) has not been discovered, and Van Dyke concludes^[6] that a second order solution for the cross-flow past an arbitrary body is not possible. However, for slender bodies of revolution at small angles of attack, the disturbances in cross-flow are much smaller than those in the axial flow; this suggests that it is more important to refine the axial flow solution than the cross-flow. Accordingly, Van Dyke proposed a hybrid solution consisting of a second order axial solution coupled with a first order solution of the cross flow. Comparisons of the hybrid theory with exact solutions by the method of characteristics have demonstrated excellent agreement, and form the basis for adoption of the hybrid theory as a sufficiently accurate solution to the potential flowfield around a projectile.

Details of First and Second Order Solutions.

For the axial flow, the discovery of the particular integral (A.26) reduces the second order problem to a sequence of two first order problems. These are solved by repeated superposition of five basic solutions, which are now derived below.

Any first order solution may be regarded as resulting from a continuous distribution of supersonic sources and sinks located along the x-axis. The function $f(\xi)$ in equation (A. 19) can be equally well represented as a continuous curve, or as the sum of a number of linear and quadratic source distributions having various strengths and starting points, as shown in Figure A-2.

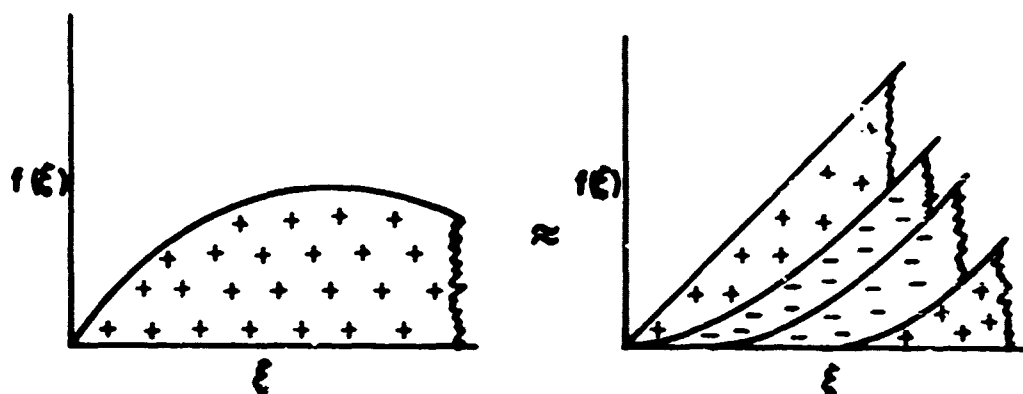


Figure A-2. Equivalent Methods of Creating a Source-Sink Distribution

The linear source distribution [$f(\xi) \sim \xi$] is required at the tip of a pointed body, since a pointed body actually produces conical flow near the apex. The use of quadratic source-sink elements [$f(\xi) \sim \xi^2$] downstream of the apex insures a smooth first order solution for evaluation of the particular integral.

If the body has continuous curvature, these two basic solutions are sufficient. However, if the body has corners or curvature discontinuities, additional solutions are required. A corner is accounted for in the first order solution by adding a square root source distribution [$f(\xi) \sim \sqrt{\xi}$] which produces a discontinuity in streamline slope along its leading Mach cone. A curvature discontinuity is accounted for by adding a three-halves power source distribution [$f(\xi) \sim \xi^{3/2}$]

which produces a discontinuity in streamline curvature along the leading Mach cone. The curvature solution is also required at a corner, since an apparent curvature discontinuity remains after the corner solution is added.

The particular integral involves derivatives of the first order solution, and therefore has stronger discontinuities. For a body curvature discontinuity, the particular integral behaves like a corner, and the corner solution must again be used. For an actual body corner, the particular integral behaves like a step in the streamlines, and an inverse square root source distribution [$f(\xi) \sim 1/\sqrt{\xi}$] must be added to cancel the apparent step.

In summary, the axial first order solution and the particular integral are calculated by superposing the five basic solutions:

- (1) Linear source solution - used at the apex of a pointed body,
- (2) Quadratic source distribution - used downstream of the apex for a body with continuous curvature,
- (3) Square root source distribution - used to account for a corner,
- (4) Three-halves power source distribution - used to account for a body curvature discontinuity,
- (5) Inverse square root source distribution - used to cancel the step in the particular integral at a corner.

Calculation of the five basic solutions is facilitated by introducing the conical variable t ,

$$t = \beta r/x. \quad (\text{A. 27})$$

Physically, t is the ratio of the tangent of the polar angle to the tangent of the Mach angle, and varies from zero on the x -axis to unity on the Mach cone.

If r is replaced by tx/β in equation (A. 19), and $f(\xi)$ is replaced by ξ^n , equation (A. 19) becomes,

$$\varphi_0(x, t) = - \int_0^{x(1-t)} \frac{\xi^n d\xi}{\sqrt{(x-\xi)^2 - t^2 x^2}} \quad (\text{A. 28})$$

Performing the indicated integrations yields the five basic axial flow solutions in the form,

(1) Linear source distribution ($n=1$)

$$\varphi_0(x, t) = -x (\text{Sech}^{-1} t - \sqrt{1-t^2}) \quad (\text{A. 29})$$

(2) Quadratic source distribution ($n=2$)

$$\varphi_0(x, t) = -\frac{1}{2} x^2 \left[\left(1 + \frac{1}{2} t^2\right) \text{Sech}^{-1} t - 3/2 \sqrt{1-t^2} \right] \quad (\text{A. 30})$$

(3) Square root source distribution ($n=\frac{1}{2}$)

$$\varphi_0(x, t) = -\sqrt{x} \frac{4\sqrt{2}}{\pi} \sqrt{1+t} (K-E) \quad (\text{A. 31})$$

where K and E are complete elliptic integrals of the first and second kind, with modulus $k = \sqrt{(1-t)/(1+t)}$.

(4) Three-halves power source distribution ($n=3/2$)

$$\varphi_0(x, t) = x^{3/2} \frac{8\sqrt{2}}{9\pi} \sqrt{1+t} [(3+t)K - 4E] \quad (\text{A. 32})$$

(5) Inverse square root source distribution ($n=-\frac{1}{2}$)

$$\varphi_0(x, t) = -\frac{1}{\sqrt{x}} \frac{2\sqrt{2}}{\pi} \frac{1}{\sqrt{1+t}} K \quad (\text{A. 33})$$

The first order solution for the cross-flow requires only two basic solutions; one for bodies having continuous curvature, and a second solution which is required only at a corner. The supersonic doublet distribution, $g(\xi)$, in equation (A. 20) is adequately represented by the sum of linear doublet elements $[g(\xi) \sim \xi]$, having various strengths and starting points. The corner solution in cross flow is represented by a square root doublet distribution $[g(\xi) \sim \sqrt{\xi}]$. If r is now replaced by tx/β in equation (A. 20), and $g(\xi)$ is replaced by ξ^m , equation (A. 20) becomes,

$$\varphi_1(x, t) = \frac{1}{tx} \int_0^{x(1-t)} \frac{(x-\xi) \xi^m d\xi}{\sqrt{(x-\xi)^2 - t \frac{x^2}{\beta^2}}} \quad (\text{A. 34})$$

Again, performing the indicated integrations yields the two basic cross-flow solutions in the form,

(1) Linear doublet distribution ($m=1$)

$$\varphi_1(x, t) = x \left[\frac{(\sqrt{1-t})}{t-t} \text{Sech}^{-1} \frac{x}{t} \right]. \quad (\text{A. 35})$$

(2) Square root doublet distribution ($m = \frac{1}{2}$)

$$\varphi_1(x, t) = \sqrt{x} \frac{2}{\beta} \frac{\sqrt{1+t}}{2} (\xi - tK). \quad (\text{A. 36})$$

Approximate Tangency Condition.

The computing scheme is simplified by using an approximate tangency condition instead of the exact condition given by equation (A. 5). In first order theory, it is consistent with the approximation already made to neglect $\varphi_{0,x}$ and $R'\varphi_{1,x}$ in comparison with unity. Similar

consistency is obtained in the second order axial solution by replacing ϕ_{0x} in equation (A. 8) with its first order counterpart, ϕ_{0x} . With these approximations, the tangency condition for first and second order solutions can be written,

$$\phi_{0r}(x, R) = R'(x). \quad (\text{A. 37})$$

$$\phi_{1r}(x, R) = 1. \quad (\text{A. 38})$$

$$\phi_{0r}(x, R) = R'(x) [1 + \phi_{0x}(x, R)]. \quad (\text{A. 39})$$

Van Dyke shows [7] that although neither exact or approximate tangency exhibits consistent superiority for smooth bodies, the use of approximate tangency invariably leads to higher accuracy in the vicinity of a corner. This result is not completely unexpected, since flow around a corner is locally a two-dimensional process, and the approximate tangency condition is known to produce more accurate velocities near corners in plane flow. The implication is that approximate tangency is consistently superior for bodies of revolution with corners; hence equations (A. 37) through (A. 39) have been adopted for calculation of flows around projectiles.

Choice of Computing Intervals.

Van Dyke has derived rules [7] for computing intervals, based on supersonic similarity. The length of the first interval, δ_0 , for a pointed body is given by,

$$\delta_0 = \frac{1}{8M \sqrt{R_0''}} (1 - \beta^2 R_0'^2). \quad (\text{A. 40})$$

Subsequent intervals are given by,

$$\delta_i = \beta R_i, \text{ for smooth bodies,} \quad (\text{A. 41})$$

and

$$\delta_c = \frac{1}{2} \beta R_c, \text{ at a corner.} \quad (\text{A. 42})$$

Van Dyke states that the relative numerical error at the end of any interval will not exceed one percent, if the previously stated interval lengths are used. Experience has demonstrated that to retain one percent accuracy throughout the flowfield, it is necessary to reduce Van Dyke's intervals by a factor of two for the first and subsequent intervals, and by a factor of four for the first interval immediately following a corner. If violent changes in body curvature occur within any given interval, the interval may have to be further reduced.